

---

# Physical interpretation of the anomalous Cherenkov rings observed with the DELPHI detector

**V. F. Perepelitsa**

ITEP, Moscow

**T. Ekelof**

Department of Physics and Astronomy, Uppsala University

**A. Ferrer**

IFIC, Valencia University

**B. R. French**

bernardfrench@bluewin.ch

## Abstract

The results of a search with the DELPHI Barrel RICH for anomalous Cherenkov rings having radii greater than those produced by ultrarelativistic particles were reported in our previous paper [1]. The search was based on the data collected by the DELPHI Collaboration at CERN during the LEP1 and LEP2 periods. A detailed study of background sources capable of producing apparently anomalous rings has been done; it indicated that the background hypothesis has a low probability ( $10^{-3}$  or less). An additional strong argument against the background hypothesis was provided by the observation of a high degree of correlation between anomalous ring radii in the liquid and gaseous radiators in the selected events. The results obtained are interpreted in this paper in terms of observation of faster-than-light particles (tachyons). In the framework of this interpretation two peaks in the tachyon mass parameter distribution are observed, at  $(0.29 \pm 0.01)$  GeV/ $c^2$  and  $(4.6 \pm 0.2)$  GeV/ $c^2$ .

This work has been performed by the authors following the rules for external access to the DELPHI archived data, as established in <http://delphiwww.cern.ch/delsec/finalrules/FINALrules011203.pdf>

The opinions, findings and conclusions expressed in this material are those of the authors alone and do not reflect in any way the views of the DELPHI Collaboration.

# 1 Introduction

We present here a physical interpretation of the anomalous Cherenkov rings that have resulted from a search for such rings in the events of  $e^+e^-$  interactions recorded in the DELPHI detector at LEP (CERN) as described in [1] (hereafter denoted by Paper I). The term “anomalous rings” stands for rings having radii greater than those produced by ultrarelativistic particles which are termed here “standard rings”. In this article standard rings are defined as having the ring radius compatible with 667 mrad in the liquid radiator and 62 mrad in the gaseous radiator, while the anomalous rings are defined as having the ring radius exceeding 700 mrad in the liquid radiator and 72 mrad in the gaseous radiator.

The results presented in Paper I are based on data consisting of ca  $10^7$  non-hadronic events collected at LEP1 and LEP2, corresponding to an integrated luminosity of  $0.76 \text{ fb}^{-1}$ . Interpreted in a straightforward way these results suggest the existence of faster-than-light particles (tachyons). Within this interpretation we provide additional information in the present paper favouring this interpretation.

Tachyons became topical some 50 years ago after being introduced to particle physics in papers [2, 3]<sup>1</sup>. Initially, the tachyon hypothesis encountered strong objections related to the principle of causality. However, it soon became clear that these objections are not valid if the existence of a preferred reference frame is assumed [5] (called the co-moving frame in relativistic cosmology), in which the distribution of the matter in the universe and the relic microwave background is isotropic, and which determines an “absolute rest frame”. In this frame the propagation of tachyons is ordered by retarded causality [6, 7, 8], i.e. that effects always follow their causes, and no causal paradoxes related to tachyons appear either in this frame or, as a consequence of the theory of relativity, in any other reference frame [9, 10, 11, 12].

If tachyons carry electric charge they are supposed to radiate Cherenkov photons [2], the Cherenkov cone angle  $\theta_c$  being related to the tachyon velocity  $\beta$  in the same way as for ordinary particles:

$$\cos \theta_c = \frac{1}{n\beta}, \quad (1.1)$$

where  $n$  is the refraction index of the medium traversed by the tachyon.

For the full description of how the anomalous rings were searched for, the reader is referred to Paper 1, which includes a description of the DELPHI experiment and its Barrel RICH detector, the event topologies studied and the cuts used to select the events, systematic effects producing hit patterns imitating anomalous rings and a detailed investigation and discussion of the different backgrounds that could fortuitously lead to the reconstruction of anomalous rings as well as the algorithm used to search for the anomalous rings. Sections 2–5 in the present paper represent an abbreviated version of the full description in Paper 1 with the purpose to provide, in the present paper, a condensed background to the interpretation given in Section 6 of the observed anomalous rings as produced by tachyons. A summary and conclusions are given in Sections 7 and 8.

There is an Appendix to the current paper which lists the constraint equations used in the kinematic fitting of the events containing anomalous rings, assuming their tachyon origin.

---

<sup>1</sup>An instructive paper by E. P. Wigner, in which faster-than-light particles also have been considered on the base of infinite-dimensional unitary irreducible representations of the Poincaré group, was published in the 1963 [4].

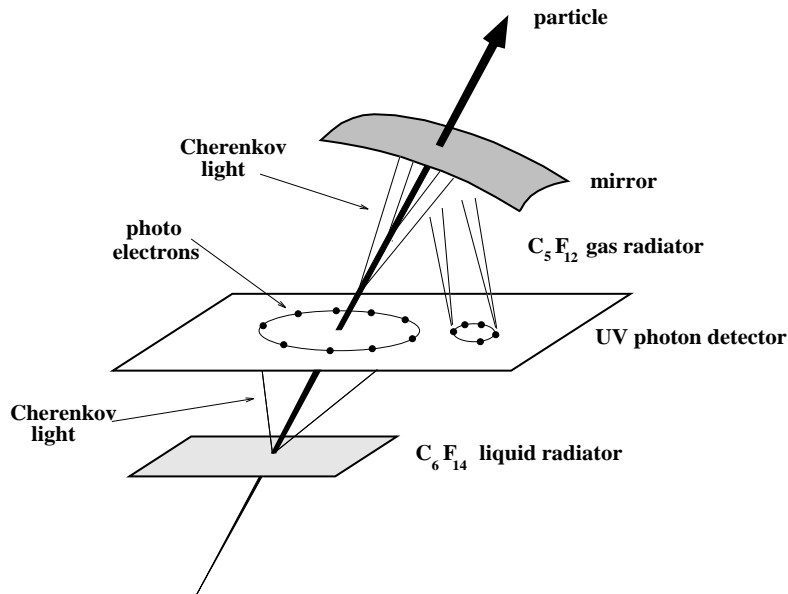
## 2 Experimental technique

The DELPHI detector is described in detail in [13, 14]. The following is a list of the subdetector units relevant for this analysis: the vertex and inner detectors (VD and ID), the main tracker (the Time Projection Chamber, TPC), the outer detector (OD), the barrel electromagnetic calorimeter (the High-density Projection Chamber, HPC), the hadronic calorimeter (HCAL), and the barrel muon chambers (MUB). In some cases the information from the small angle tile calorimeter (STIC) was also used.

The principal detector used in this analysis was the barrel Ring Imaging Cherenkov detector (Barrel RICH).

The DELPHI Barrel RICH is described in detail in [15, 16, 17, 18, 19]. It contained two radiators, the liquid radiator ( $C_6F_{14}$ , refraction index  $n = 1.273$ ) and the gaseous radiator ( $C_5F_{12}$ ,  $n = 1.00194$ ). The Cherenkov photons from these two radiators were detected by TPC-like photon detectors consisting of 24 pairs of quartz drift tubes (drift boxes), covering a full azimuthal range with 24 Barrel RICH sectors, extended to  $\pm 155$  cm from the mid-wall. The drift gas (75% methane  $CH_4$  and 25% ethane  $C_2H_6$ ) was doped with 0.1% of the photosensitive agent TMAE, by which the ultraviolet Cherenkov photons were converted into single free photoelectrons, the mean photon conversion length being equal to 1.8 cm. The TMAE photo-ionization threshold of 5.63 eV and the transmission cut-off of the liquid radiator and drift tube quartz windows of 7.50 eV limited the photon wavelength detection range to the band of 165 - 220 nm.

The principles of the creation of Cherenkov ring images in both radiators of the DELPHI Barrel RICH are illustrated in the following figure:



The rings formed by the hits of photons originating from a given radiator were distinguished by the location of the hits in two different parts of the drift boxes, separated by the box median plane, the inner part for the liquid and outer part for the gaseous radiators (in the present paper “inner” and “outer” positions in the DELPHI detector is with respect to the colliding beam axis).

The standard ring radii in the liquid and gas radiators, expressed in angular units, were 667 and 62 mrad, respectively. The total single photon standard error of the liquid radiator  $\sigma_{p.e}$  was 18-28 mrad for standard rings. Each sector of the gaseous radiator was equipped

with six parabolic mirrors distributed along the  $z$  axis <sup>2</sup>, which focused the Cherenkov photons generated in the radiator volume back onto the photon detector. The gas radiator single photon standard error  $\sigma_{p.e.}$  was about 4 mrad for small radius anomalous rings, increasing by an order of magnitude for very big rings due to geometric aberrations intrinsic to parabolic mirror optics. With the average Cherenkov photon numbers per standard ring of 14 and 8 [14] <sup>3</sup> for the liquid and gaseous radiators, respectively, the Cherenkov cone angular error  $\sigma$  for the rings associated with high momentum hadronic tracks was about 9 mrad for the liquid radiator and about 2.7 mrad for the gaseous radiator [20].

After the processing of the raw data with the use of the DELPHI general pattern recognition package *DELANA* [14] to produce the DELPHI data summary tapes (DST's), the RICH data for each individual track consisted of photon trajectories starting on track segments inside a given radiator volume, and terminating inside the RICH drift boxes on hits detected in the latter. This information was treated rather differently in the standard DELPHI analysis and in the analysis presented here.

The DELPHI standard way was to use the reconstructed Cherenkov angles to identify the particle producing the track by applying the maximum likelihood technique [14]. Five mass hypotheses ( $m_e$ ,  $m_\mu$ ,  $m_\pi$ ,  $m_K$ ,  $m_p$ ) were tried and the results were used to identify the particle. Additionally, an independent estimation of the ring radii relevant to each charged particle traversing the RICH was made and the results were stored on the DST's [20], including the averaged Cherenkov angle, the number of photoelectrons in the ring, an estimation of the background, etc., together with information on individual hits, and these data were used in this analysis as described below. Unfortunately, for the present investigation, the hits which could correspond to Cherenkov angles exceeding certain limits were not retained in this procedure, these limits being 750 mrad for the liquid radiator and 102 mrad for the gaseous one. The information about these large angle hits is not available on any of the types of DELPHI DST's. This obviously restricted the power of the preliminary selection of events containing anomalous rings at the DST level. Such a selection, described in Sect. 4, was based on other event signatures, though the information about Cherenkov angles within the limits mentioned above was used in part for the selection, as will be further explained.

The events tagged by this preliminary selection were reprocessed, and the RICH data in them were treated following a procedure specially developed for the present analysis. It starts with an analysis of the information stored in raw data tapes extracted by the DELPHI event server. Then several steps of the standard procedure, described above, are performed, to reconstruct the Cherenkov photon directions with respect to tracks, however without any restrictions on the radiation angles. After this the photon directions were projected, as described below, onto the plane perpendicular to the track trajectories in the corresponding radiator which will here be called the Cherenkov plane. The coordinate frame in this plane has its origin at the position of the center of the expected ring as reconstructed from the track parameters. The plane coordinates  $x, y$  of the photon projections, expressed in angular units, are calculated from the polar and azimuthal angles of the Cherenkov photons,  $\theta_c$  and  $\phi_c$ :  $x = \theta_c \sin \phi_c$ ,  $y = \theta_c \cos \phi_c$ . The resulting hit pattern, which as a rule is contaminated by random background hits, constitutes the

---

<sup>2</sup>In the DELPHI reference frame the  $z$  axis is along the direction of the  $e^-$  beam. It defined the particle polar angles  $\Theta$ , while the particle azimuthal angles  $\Phi$  were defined in the  $xy$  plane.

<sup>3</sup>These numbers reduce to 9 and 5, respectively, within  $\pm 1\sigma_{p.e.}$  cited above.

input to the search for Cherenkov rings. The ring search algorithm combined with the method of evaluation of the probability that the rings are due to background fluctuations, that fortuitously lead to the reconstruction of ring images, is described in [1]. Only the rings having the background probability below 10% were kept for further consideration.

In order to illustrate the above procedure several anomalous rings found with it are shown in Figs. 1-6.

### 3 Event topologies studied

In selecting the events for our analysis we followed the predictions for tachyon behaviour in an experimental set up [21] based on expected tachyon characteristics [11]. In particular, it is important to account for selection rules based on the angular momentum conservation as they are predicted to affect the production and propagation (through the medium) of tachyons with non-zero spin (helicity), while scalar tachyons are expected to be excluded on the theoretical ground [11].

*Topology 1. Coupled tachyon-antitachyon pair production associated with a high energy photon.* The simplest topology to produce non-zero helicity tachyons in  $e^+e^-$  interactions, which is free of selection rules due to angular momentum conservation seems to be the reaction

$$e^+e^- \rightarrow \gamma t^+t^-, \quad (3.1)$$

where  $\gamma$  denotes a high energy photon and  $t^+, t^-$  stand for a pair of charged tachyons, produced with a vanishingly small opening angle, the photon and the pair going in opposite directions. Whatever would be (non-zero) helicities of the tachyon and the antitachyon, their angular momenta can compensate each other, and no appreciable suppression of the tachyon production by the selection rules mentioned above can be expected in this case. Schematically, this topology can be presented by a diagram shown in Fig. 7a (the dashed lines in it represent the particles which go undetected; in the case under consideration these are beam particles). In the case when two charged tachyons are non-resolved by the TPC the common tachyon track can be distinguished by anomalously high ionization loss ranging from single to double electron ionization response, with the most probable value being that of double ionization. This expectation follows from kinematic considerations: in order to produce an identifiable intermediate ionization response at least one of two tachyons has to possess a velocity exceeding, say,  $1.1c$ . This is not very probable if the tachyon mass parameters are of the order of several  $\text{GeV}/c^2$  or less. The typical particle energies at LEP in the events of low multiplicity are higher than 10 GeV, and being shared by tachyons they would ensure tachyon velocities very close to  $c$ .

Two respective examples of topology 1 candidate events are given in Figs. 8-12.

*Topology 2. Back-to-back (or quasi-back-to-back) tachyon-antitachyon production.* Under certain conditions a tachyon-antitachyon pair can be produced alone in an  $e^+e^-$  collision:

$$e^+e^- \rightarrow t^+t^-. \quad (3.2)$$

with the two tachyons going in opposite directions. Such a reaction is allowed only if the tachyons have the minimal possible helicity values,  $1/2$  (excluding the possibility of scalar charged tachyons on theoretical grounds, as mentioned above). The reaction diagram of

this process is presented in Fig. 7b. Such a process is, from the point of view of the angular momentum conservation, analogous to an anti-neutrino scattering on an electron. The distribution of the production angle of tachyon pair  $\Theta$  is expected in this case to be proportional to  $\cos^2 \Theta$ , i.e. rather suppressed in the barrel region, vanishing at  $\Theta = 90^\circ$ .

The situation with the angular momentum conservation can be softened in the case of tachyon pair production in  $\gamma\gamma$  interactions, i.e. in reaction

$$e^+e^- \rightarrow e^+e^- t^+t^-. \quad (3.3)$$

in which tachyon configuration can be defined as quasi-back-to-back one (the final faster-than-light particles are acollinear but coplanar). The diagram of this reaction is shown in Fig. 7c. As can be seen comparing this diagram with the diagram of reaction (3.2), these two reactions, in spite of being quite different in terms of the tachyon production mechanism, generate the same two-track, (quasi-) back-to-back topology. This topology is similar to the Bhabha-like event topology in the case of reaction (3.2), or to the  $e^+e^-$  pair production via  $\gamma\gamma$  interaction in the case of reaction (3.3). Thus the Bhabha-like and  $\gamma\gamma$  events are expected to be the main source of background events in this channel. The decisive signature of the events of reactions (3.2) and (3.3) has to be the observation of anomalous rings in the RICH detector associated with both candidates for tachyon tracks, and a successful passage of an appropriate kinematic treatment by the events. Two respective examples of topology 2 event candidates are shown in Figs. 13-16.

*Topology 3. Electroproduction of a tachyon-antitachyon pair in front of the TPC.* The suppression of the tachyon production by selection rules due to the angular momentum conservation can be essentially weakened if a tachyon-antitachyon pair is created in matter, in which case some additional angular momentum degrees of freedom can appear. Such a process could be induced, for example, by secondary electrons (or positrons), generated in the beam-beam or  $\gamma\gamma$  interactions, when these particles pass through the detector material, with the following reaction taking place:

$$eX \rightarrow X'e t^+t^-, \quad (3.4)$$

where  $X$  and  $X'$  denote a charged object (most probably, a nucleus of the detector medium with which the incident electron interacts<sup>4</sup>), before and after the interaction. Excepting this charged object, there are no undetectable charged particles in this reaction (see the reaction diagram in Fig. 7d). Thus a typical topology of events of this kind would be a presence of a “jet” consisting of three tracks, of which at least two have non-zero impact parameters with respect to the primary vertex. The particle producing the three-particle jet is expected to be opposed by another track in the opposite hemisphere, as shown in an example of this topology event candidate in Figs. 17, 18.

---

<sup>4</sup>Due to a big tachyon longitudinal extension, which accordingly to [11] should essentially exceed a nuclear scale, the coherent electroproduction of tachyons on nuclei is expected to dominate this process.

## 4 Selection of events having candidate anomalous rings

The following selection cuts were applied for the preliminary selection of events from the DELPHI DST's:

*The general selection of events* was done vetoing the hadronic events defined according to the DELPHI “Team 4” criteria [14]<sup>5</sup>. This retained about  $10^7$  events (called “quasi-leptonic events”), found in the 1992 - 2000 data<sup>6</sup>. A further reduction of the amount of hadronic events was performed by using the DELPHI electromagnetic calorimeter as described below. Muons were identified (and rejected) with the HPC, HCAL and MUB responses. Another general selection criterion was the requirement that for all tracks of the events the errors of the momenta derived from the curvature of the tracks be below certain limits ( $\delta p/p < 0.3$ ). The tracks were furthermore required to be within the geometrical acceptance of the gas radiator of the DELPHI Barrel RICH ( $46^\circ < \Theta < 134^\circ$ ), with the barrel RICH being in an operational state.

The further selection of events used the cuts designed to enhance the contents of events of topologies 1, 2 and 3 which are described below (the term *jet* here corresponds to a single neutral or charged particle or two or three tightly bunched charged particles), and the results of the application of these selections to the DELPHI DST data is shown in Tables 1 and 2 of Paper I.

### 4.1 Topology 1

1. Two jets in the opposite hemispheres are required in the event: one neutral jet and one jet consisting of 1 or 2 charged particles; each of the jets should have at least 50% of the beam energy.
2. Track(s) of the charged jet should have associated shower(s) in the HPC with the total jet shower energy exceeding half of the jet momentum, the number of active HPC layers in the shower(s) being greater than or equal to 5 (of 9).
3. Track(s) of the charged jet should have the first measured point(s) in the first layer of the DELPHI vertex detector (VD).
4. In the case of a single-track charged jet (topology 1a) the track ionization has to be within the limits of  $2.0 < dE/dx < 3.8$  mips<sup>7</sup> (corresponding to the 2 charged tracks being non-separable in the TPC), with the number of TPC wires available for ionization measurement exceeding 40 out of a total of 192 wires (this cut aimed at the suppression of Compton event background).
5. In the case of a jet with two separated tracks (topology 1b) the jet mass, calculated under hypothesis of the electron mass for the tracks, has to be below  $0.5 \text{ GeV}/c^2$ ,

---

<sup>5</sup>The main criterion for selecting hadronic events was the requirement of a multiplicity above 4 of charged particles with  $p > 400 \text{ MeV}/c$ ,  $20^\circ < \theta < 160^\circ$  and a track length of at least 30 cm in the TPC, with a total energy in these charged particles above  $0.12 \times E_{cm}$ .

<sup>6</sup>The transition from LEP1 to LEP2 took place in the year 1995. LEP1 beam energies were centered around the mass of  $Z^0$ -boson ( $91.2 \text{ GeV}/c^2$ ), the LEP2 period was aimed at physics beyond  $Z^0$ , with beam energies spanning between 161 and 208 GeV (the averaged energy being 196 GeV).

<sup>7</sup>A mip is the  $dE/dx$  of a minimum ionization particle.

and the smaller of the two track momenta has to exceed  $4 \text{ GeV}/c$ <sup>8</sup>. To suppress the Compton event background the jet acollinearity was required to be below  $2^\circ$ .

It is worth to note that for a proper finding of Cherenkov rings (standard or anomalous ones) only the track direction in the RICH, and not its momentum value, is required. This direction is considered to be well defined even for the events in which two tracks were not separated (not resolved) in the TPC, identified by double ionization only (the tracks from point 4 above). The reason for that these tracks were not resolved in the TPC was, in an addition to their negligible opening angle, their high momenta leading to a small curvature of their trajectories in the DELPHI detector magnetic field. This resulted in the appearance of these tracks as practically straight lines in the detector; these tracks produced two Cherenkov rings in each of the RICH (liquid and gaseous) radiators (in the case of electron tracks all the rings are standard).

## 4.2 Topology 2

1. Two tracks of opposite charge are required in a 2-jet event, one track per jet, both tracks having momenta greater than  $4 \text{ GeV}/c$ . Each jet should have at least 60% of the beam energy (topology 2a, Bhabha-like events) or, alternatively, each jet should have less than 60% of the beam energy (topology 2b,  $\gamma - \gamma$  events).
2. Both tracks of the event should have associated showers in the HPC with each shower energy exceeding half of the track momentum, the number of active HPC layers in the showers being greater than or equal to 5 (of 9).
3. The tracks have to go in opposite directions in the  $xy$  plane having the track acollinearity lower than  $2^\circ$  (in the case of topology 2a) or, in the case of topology 2b, having the track acollinearity higher than  $2^\circ$  and the track acoplanarity below  $4^\circ$ .
4. Each of the tracks should have a gas Cherenkov angle, stored on the DST, within the region 72 to 102 mrad<sup>9</sup>, with at least 5 photoelectrons associated with each ring;
5. or, alternatively, one of the two tracks should have a Cherenkov angle within the region 80 to 102 mrad, with at least 5 associated photoelectrons.

## 4.3 Topology 3

1. Two jets are required in the event: one jet consisting of a single track, and the other consisting of 3 charged particles, with the overall sum of the track charges equal to zero. All the tracks in the 3-particle jet should have momenta exceeding  $3 \text{ GeV}/c$ .
2. Tracks in the 3-particle jet should have associated showers in the HPC with each shower energy exceeding half of the track momentum, the number of active HPC layers in the showers being greater than or equal to 5 (of 9).

---

<sup>8</sup>This cut was applied in order to keep the efficiency of the track association with its HPC shower close to 100%.

<sup>9</sup>The upper limit is defined by a restriction on the gas Cherenkov radii imposed when producing the DST's.

3. For a primary suppression of  $\tau - \tau$  events (abundant in LEP1 data set) the effective mass of charged particles in the 3-particle jet (calculated prescribing pion masses to the tracks) is demanded to be greater than  $0.5 m_\tau$  ( $0.89 \text{ GeV}/c^2$ ), and the jet momentum is required to be greater than 0.8 of the beam momentum.
4. Two tracks in the 3-particle jet are required to have the first measured point at the detector radius  $R > 35 \text{ cm}$  (i.e. outside the ID, the DELPHI Inner Detector). And at least one track in this jet should have an impact parameter with respect to the primary vertex in the  $xy$  plane exceeding 6 mm, or two tracks should have impact parameters each exceeding 4 mm, while the impact parameters of all tracks with respect to the primary vertex should be below 10 cm.
5. At least two tracks in the three-track jet should have a non-standard RICH response from the gas radiator (stored on the DST), i.e. either ring radii outside of the standard ring limits of  $52 < r < 72 \text{ mrad}$ , or no response at all <sup>10</sup>, while each track is required to have some response from the liquid radiator; these tracks should be within the angular acceptance of the gas radiator i.e. within the range of  $46^\circ < \Theta < 134^\circ$ .

#### 4.4 Final selection

The cuts described in Sects. 4.1 to 4.3 resulted in the selection of 395 events as primary signal candidate events of topologies 1, 2 and 3 (which correspond to the sum of events in the Selection 4 row of Tables 1 and 2 in Paper I.

A further analysis of all the selected events was done retrieving these events from the DELPHI raw data using the DELPHI event server, reconstructing the Barrel RICH hit patterns for all tracks in these events and searching for anomalous rings associated to each track, as described in Appendix 1 of Paper I.

Of the 395 selected events 53 events were found to have at least one anomalous ring with a probability to be composed of background hits below 10%; the distribution of these events over different topologies is shown in Selection 5 rows of Tables 1 and 2 of Paper I. The minimal number of photons per ring was required to be 4. In addition, the events of topologies 1 and 2 were required not to have standard rings in the gas radiator.

Of these 53 events 29 events were found to possess two gaseous anomalous rings (at least one anomalous ring per track in topology 2). All these events were subjected to a further treatment, aimed at the finding of rings, standard and/or anomalous, in the liquid radiator. The search for liquid radiator rings in the events with the found gas rings, combined with the method of evaluation of the probability that the ring is composed of background hits, was performed as described in Appendix 2 of Paper I. The range of the liquid ring radii searched for with this method spanned between 600 and 1100 mrad. In the case of such a ring being found with the ring radius exceeding 700 mrad (excluding quartz ring range, 857 - 909 mrad) it was considered as an anomalous liquid radiator ring; only those anomalous liquid radiator rings having the background probability below 10% were accepted for further analysis. Then the background probabilities of all anomalous rings in a given event were multiplied, and the product of the probabilities was required

---

<sup>10</sup>This non-standard response was expected in the cases of anomalous rings having radii greater than 102 mrad.

to be less than  $10^{-3}$ . Of the selected 29 events this left 9 events of topology 1, 6 events of topology 2, and 12 events of topology 3, in total 27 events as given in the Selection 6 rows in Tables 1 and 2 of Paper I. None of the anomalous rings in these events were compatible with being due to the systematic effects described in Section 5 of Paper I. The characteristics of the rings contained in all the 27 selected events are given in Tables 3 to 5 of Paper I.

The studies of backgrounds and possible systematic effects, which can lead to the appearance of spurious anomalous rings, are described in detail in Sects. 6 to 9 of Paper I. It follows from these studies that the probability that the events with the observed anomalous rings can be explained by known physical processes is very low (below  $10^{-9}$ ). Moreover, the comparison of the rates of events with single and double anomalous rings, carried out in Sect. 8 of Paper I, indicated a clear tendency for the observed anomalous rings to be produced in pairs.

## 5 Correlation between gaseous and liquid radiator rings

An important feature of the DELPHI RICH was the presence of two radiators: the liquid radiator and outside it, the gaseous one. With the use of the relationship originating from Cherenkov formula

$$n_{liq} \cos \theta_{liq} = n_{gas} \cos \theta_{gas}, \quad (5.1)$$

the ring radius expected in the liquid radiator can be derived from the gaseous ring radius and *vice versa*.

Fig. 19 shows the anomalous ring radii observed in the gas radiator plotted against the ring radii observed for the same track in the liquid radiator for 27 events listed in Tables 1, 2 and 3 of Paper I, showing a clear correlation between the radii. The curved line in the figure is not a fit to the data, but has been derived using the relation (5.1) with  $n_{liq} = 1.273$  and  $n_{gas} = 1.00194$ .

The same correlation, presented in terms of particle velocities as calculated from the ring radii in both radiators according to formula (1.1),  $\beta_{liq}$  and  $\beta_{gas}$ , is shown in Fig. 20. The correlation coefficient calculated for 53 points of Fig. 20 equals 0.992. The probability of obtaining such a coefficient for uncorrelated variables was estimated on the basis of an analysis of  $10^9$  MC “toy experiments” in each of which the values of the 53 velocity pairs,  $\beta_{liq}$  and  $\beta_{gas}$ , were generated as distributed randomly according to the corresponding projections of the plot in Fig. 20. The probability resulting from this analysis is  $10^{-9}$ .

The sum of  $\chi^2$  for deviations of 53 points in Fig.20 from the main diagonal is 40.1. The corresponding probability for that these points are in agreement with the predictions of formula (5.1) is near 95%.

## 6 Kinematic treatment of events containing anomalous rings

This analysis consisted of the following two-step procedure.

First, the momentum  $p$  of a tachyon is derived from the information provided by the DELPHI tracking devices. Since a tachyon is a space-like particle, the square of its 4-momentum  $P$ ,  $P^2 = E^2 - p^2 = -\mu^2$ , is negative, where  $E$  is the tachyon energy and  $\mu$  is the tachyon mass parameter. The velocity of the tachyon is defined as for ordinary particles to be  $\beta = p/E, \beta > 1$ . Using the measured Cherenkov angle  $\theta_c$  to determine the velocity from relation  $\beta = 1/n \cos \theta_c$  one obtains the following expression for the tachyon mass parameter:

$$\mu = \frac{p}{c} \sqrt{1 - (n \cos \theta_c)^2} \quad (6.1)$$

where  $n$  is the refraction index of the corresponding radiator. The distributions of mass parameters calculated with formula (6.1) for tachyon track candidates are shown in Fig. 21a, b, separately for regions of low and high mass parameter values. One can see that there are two clusters of entries grouping around  $0.28 \text{ GeV}/c^2$  (Fig. 21a) and  $5 \text{ GeV}/c^2$  (Fig. 21b).

Then for those events which have both momenta of tachyon track candidates reconstructed by DELANA (always of opposite electric charge) we plot, in Figs. 21c, 21d, a two-dimensional distributions of mass parameters of the tachyon track candidates. One can see that the two clusters of entries mentioned above can be seen in this figure are present also, having the cluster centers close to the diagonal of the plot. Moreover, a third cluster consisting of 5 events around  $1 \text{ GeV}/c^2$  can be seen in this plot. The correlation coefficient calculated for 19 points on the plot in Fig. 21d equals to 0.970. The probability of obtaining such a high coefficient for uncorrelated mass parameters was estimated to be below  $10^{-6}$ . This estimation is based on the analysis of  $10^7$  MC “toy experiments”, in each of which the values of 19 mass-parameter pairs were generated as distributed randomly within the ranges of the axes of Fig. 21d.

This result is interpreted as an indication for mass parameters of the tachyon and the antitachyon candidates produced in a given event to be of equal value. This indication, together with the formal arguments in [4] for the tachyon and antitachyon mass parameters to be equal, was used as an argument to keep the mass parameter values equal in the further kinematic treatment of each of selected tachyon candidate event.

This further treatment was based on an over-constrained kinematic fit of the event variables, i.e. with the number of constraint equations exceeding the number of unknowns. These equations are listed in the Appendix of this paper. Four equations based on energy-momentum conservation (equations A.1-4 and A2.1-4 in the Appendix) plus two or more equations based on Eq. 6.1 (equations A1.5-6 and A2.5-6 in the Appendix), one for each anomalous ring found in a given event, were used in the fit. In the events of topology 1a, in which tachyon track candidates were not resolved in the TPC, an additional constraint equation was implied using the  $dE/dx$  information from the common tachyon-antitachyon track candidate (equation A1.7 in the Appendix – for this is used that the  $dE/dx$  for tachyons is assumed to be equal to that the Fermi plateau for  $\beta \rightarrow 1$  and decrease with increasing  $\beta$  above 1 like  $1/\beta^2$ , see ref. 21, p. 6).

The unknowns were the tachyon mass parameter  $\mu$ , assumed to be equal for the tachyon and antitachyon, and for topology 1a the energy of the tachyon whose momentum was not measured. In the events of this topology and of topology 1b an additional unknown, the energy of an initial state radiation (ISR) photon, was treated in the case of the acollinearity of the tachyon-antitachyon candidate pair with the high energy photon detected in a given event exceeded  $1^\circ$  (which would correspond to the ISR photon energy exceeding  $1.5 \text{ GeV}$ ). In the events of topology 2, reaction (3.3), instead of this unknown

two other additional unknowns were treated, the algebraic sum of momenta of the final state  $e^+e^-$  and their invariant mass.

The events of topology 3 41633:1568, 104949:27827 and 105892:13127, having visible energy compatible with the beam  $e^+e^-$  pair  $\sqrt{s}$  and the jet acollinearity below  $1^\circ$ , were treated as events of topology 1 (without the ISR photon)<sup>11</sup>. In the remaining events of this topology the over-constrained kinematic fit was built over constraint equations using the Cherenkov angles of the anomalous rings found in these events, the number of unknowns being one, namely, the tachyon mass parameter (common for both tachyon track candidates). The fit results are given in Tables 1 -3, together with some input kinematic parameters, including measured radii of the anomalous Cherenkov rings and their errors. Also the number of degrees of freedom of the kinematic fit in a given event is shown. We give no post-fit errors of the measured parameters in the tables since they are in most cases practically equal to the input errors, only slightly decreased by the fit.

The distributions of fitted mass parameters are shown in Fig. 22. The peaks in these distributions were fitted with Gaussians. In the low mass region the Gaussian mean value equals to  $(0.290 \pm 0.005)$  GeV/ $c^2$  with the standard deviation (width) of  $(0.012 \pm 0.004)$  GeV/ $c^2$ . In the high mass region the Gaussian mean value equals to  $(4.55 \pm 0.12)$  GeV/ $c^2$  with the standard deviation of  $(0.40 \pm 0.12)$  GeV/ $c^2$ . In the both cases the peak widths are compatible with the accuracy of the determination of the tachyon mass parameter in the appropriate mass region. Note also the cluster of 5 events spread about the tachyon mass parameter of 0.9 GeV/ $c^2$ .

## 7 Summary

- 1). The observation of particle trajectories producing Cherenkov rings with radii significantly exceeding the standard ones (produced by ultrarelativistic particles) is interpreted as evidence for the existence of tachyons, i.e. particles travelling faster than light.
- 2). The studies of backgrounds and possible systematic effects, which can lead to the appearance of spurious anomalous rings, were carried out as described in Paper I and have shown that the probability that the events with the observed anomalous rings can be explained by known physical processes is very low ( $10^{-3}$  or less). Moreover, a comparison of rates with a single and double gaseous anomalous rings indicates a clear tendency for the observed anomalous rings to be produced in pairs.
- 3). In all the cases when anomalous rings associated with a given track are observed in both the liquid and the gaseous radiators, the ring radii are highly correlated according to the respective refractive indices of these radiators (see formula (5.1) and Figs. 19 and 20). The correlation coefficient for the points in Fig. 20 is high (0.992) and the probability to obtain such a correlation coefficient for uncorrelated data is low (estimated to be below  $10^{-9}$ ).

---

<sup>11</sup>There was an exceptional event (114204:2668) of this topology in which both tachyon candidate tracks were badly measured, which together with other kinematic uncertainties of this event prevented a kinematic fit. The event 79940:2890 was fitted with 1 kinematic equation (instead of 4), using the energy conservation for the 3-particle jet ( $e^-t^+t^-$ ), with the jet shower energy measured by the HPC.

- 4). For tachyon track candidates, associated with anomalous rings and having well measured momenta, the tachyon mass parameter can be calculated using formula (6.1). The calculated masses group around 0.28 and 5 GeV/ $c^2$  (see Fig. 21a, b). In the events when both tachyon track candidates have measured momenta (always of opposite sign) the calculated masses group around the main diagonal of the 2-dimensional mass distributions (see plots 21c, 21d), which indicates the tachyon-antitachyon mass parameter equality predicted by the theory [4] (see also [11]). Correlation coefficient for the points on the plot 21d equals to 0.970. The probability of obtaining such a correlation coefficient for uncorrelated mass parameters is below  $10^{-6}$ .
- 5). 26 of the 27 selected events successfully passed the over-constrained kinematic fits based on the tachyon production hypothesis for these events. The distributions of the tachyon mass parameters of the fitted events (Fig. 22) show two peaks against the vanishing background at tachyon mass parameters of 0.29 and 4.5 GeV/ $c^2$ , with the peak widths being compatible with the expected tachyon mass parameter determination accuracy in the appropriate mass regions.

## 8 Conclusion

An analysis of events with anomalous Cherenkov rings in the DELPHI Barrel RICH has been made under the hypothesis that these rings result from the radiation of faster-than-light particles, i.e. tachyons.

A detailed study of backgrounds carried out in the Paper I indicates that the probability that the reconstructed rings are the result of fortuitous combinations of background hits is low. An argument against the background hypothesis is provided by the observation of a high correlation between anomalous ring radii found in the liquid and gas radiators seen in Figs. 19, 20.

In the framework of the tachyon interpretation of the particles associated to the observed anomalous rings and assuming the equality of the tachyon and antitachyon mass parameters indicated by the mass correlation plot shown in Fig. 21d) an over-constrained kinematic fit of 26 of 27 selected events could be tried. The distributions of the tachyon mass parameters derived from the fit is narrowly peaked at two mass values, at  $0.290 \pm 0.005$  GeV/ $c^2$  and  $4.55 \pm 0.12$  GeV/ $c^2$  with little background, displayed in Fig. 22.

Our conclusion is that further searches for the faster-than-light particles should be made in dedicated experiments in order to corroborate or refute the findings of this analysis.

One can use for the tachyon search the existing data of past and current experiments, e.g. the data of the ALICE experiment at LHC which contains a RICH (called HMPID) and a TOF system, the latter with a declared resolution of 80-120 ps [22]. The optimal processes for the investigation could be  $\gamma\gamma$  interactions (corresponding to our topology 2, reaction 3.3), with an expected  $Z^2$  enhancement factor for the tachyon production in Pb-Pb collisions. The data of the LHCb experiment [23] which contains RICH detectors with a high Cherenkov angle resolution [24] also can be used selecting low multiplicity events in the data of pp, pPb and Pb-Pb collisions.

## Acknowledgments

We are greatly indebted to the DELPHI Collaboration for the permission to use the DELPHI experiment data in our analysis.

We thank Profs. Yu. G. Abov, K. G. Boreskov, F. S. Dzheparov, O. V. Kancheli, A. M. Kunin and Drs. F. Dydak, O. N. Ermakov, A. I. Golutvin, A. A. Grigoryan, S. Sila-Novitsky for fruitful discussions and Drs. U. Schwickerath and R. M. Shahoyan for technical assistance.

# Appendix. Constraint equations of kinematic fits

## Topology 1

Definitions:

- $p_{t1}$  - measured tachyon candidate 1 track momentum;
- $\Theta_{t1}$  - measured common tachyon candidate pair polar angle;
- $\Phi_{t1}$  - measured common tachyon candidate pair azimuthal angle;
- $E_\gamma$  - measured HE photon energy;
- $\Theta_\gamma$  - measured HE photon polar angle;
- $\Phi_\gamma$  - measured HE photon azimuthal angle;
- $\Theta_{ISR}$  - ISR photon polar angle  $\Theta$ : measured by the STIC or, otherwise, put to  $0^\circ$  or  $180^\circ$ <sup>12</sup>;
- $\Phi_{ISR}$  - ISR photon azimuthal angle  $\Phi$ : measured by the STIC or, otherwise, put to  $0^\circ$ ;
- $R_{t1}$  - measured radius of the anomalous ring associated with the tachyon candidate 1;
- $R_{t2}$  - measured radius of the anomalous ring associated with the tachyon candidate 2;
- $n_1$  and  $n_2$  - refraction indices of the radiators in which the corresponding rings were found;
- $\rho$  (in the case of topology 1a) - measured common tachyon candidate track  $dE/dx$  reduced by the Fermi plateau value (1.60 mips in the DELPHI TPC);
- $\mu$  - unknown (common) tachyon mass parameter;
- $\tau_{ISR}$  - unknown ISR photon energy;
- $E_{t2}$  - unknown energy of the second tachyon in the case of topology 1a;
- $p_{t2}$  - momentum of the second tachyon: measured in the case of topology 1b, otherwise equal to  $\sqrt{\mu^2 + E_{t2}^2}$ ;
- $\epsilon_{t2}$  - energy of the second tachyon: unknown ( $E_{t2}$ ) in the case of topology 1a, otherwise equal to  $\sqrt{p_{t2}^2 - \mu^2}$ ;
- $E_{c.m.s.} = \sqrt{s}$ .

Equations:

$$f_1 = (p_{t1} + p_{t2}) \sin \Theta_{t1} \cos \Phi_{t1} + E_\gamma \sin \Theta_\gamma \cos \Phi_\gamma + \tau_{ISR} \sin \Theta_{ISR} \cos \Phi_{ISR} = 0 \quad (\text{A1.1})$$

$$f_2 = (p_{t1} + p_{t2}) \sin \Theta_{t1} \sin \Phi_{t1} + E_\gamma \sin \Theta_\gamma \sin \Phi_\gamma + \tau_{ISR} \sin \Theta_{ISR} \sin \Phi_{ISR} = 0 \quad (\text{A1.2})$$

$$f_3 = (p_{t1} + p_{t2}) \cos \Theta_{t1} + E_\gamma \cos \Theta_\gamma + \tau_{ISR} \cos \Theta_{ISR} = 0 \quad (\text{A1.3})$$

$$f_4 = \sqrt{p_{t1}^2 - \mu^2} + \epsilon_{t2} + E_\gamma + \tau_{ISR} - E_{c.m.s.} = 0 \quad (\text{A1.4})$$

$$f_5 = \sqrt{p_{t1}^2 - \mu^2} / p_{t1} - n_1 \cos R_{t1} = 0 \quad (\text{A1.5})$$

$$f_6 = \epsilon_{t2} / p_{t2} - n_2 \cos R_{t2} = 0 \quad (\text{A1.6})$$

In the case of topology 1a:

$$f_7 = (1/\beta_{t1}^2 + 1/\beta_{t2}^2) - \rho = 1 - \mu^2/p_{t1}^2 + \epsilon_{t2}^2/p_{t2}^2 - \rho = 0, \quad (\text{A1.7})$$

where  $\beta_{t1}$  and  $\beta_{t2}$  are velocities of the tachyons 1 and 2 defined by gas rings, [21], p. 6.

## Topology 2

Definitions:

- $p_{t1}$  - measured tachyon candidate 1 track momentum;

---

<sup>12</sup>The choice between  $0^\circ$  and  $180^\circ$  was definite, requiring the positivity of the ISR photon energy,  $\tau_{ISR} > 0$  ( $\tau_{ISR}$  to be defined below).

$\Theta_{t1}$  - measured tachyon candidate 1 track polar angle;  
 $\Phi_{t1}$  - measured tachyon candidate 1 track azimuthal angle;  
 $p_{t2}$  - measured tachyon candidate 2 track momentum;  
 $\Theta_{t2}$  - measured tachyon candidate 2 track polar angle;  
 $\Phi_{t2}$  - measured tachyon candidate 2 track azimuthal angle;  
 $\Theta_{ee}$  - polar angle of the final  $e^+$ ,  $e^-$  summary momentum: measured or, otherwise, put to  $0^\circ$  (not necessary in the case of topology 2a);  
 $\Phi_{ee}$  - azimuthal angle of the final  $e^+$ ,  $e^-$  summary momentum: measured or, otherwise, put to  $0^\circ$  (not necessary in the case of topology 2a);  
 $R_{t1}$  - measured radius of the anomalous ring associated with the tachyon candidate 1;  
 $R_{t2}$  - measured radius of the anomalous ring associated with the tachyon candidate 2;  
 $n_1$  and  $n_2$  - refraction indices of the radiators in which the corresponding rings were found;  
 $\mu$  - unknown (common) tachyon mass parameter;  
 $p_{ee}$  - the algebraic sum of the final  $e^+$ ,  $e^-$  momenta (zero in the case of topology 2a);  
 $m_{ee}$  - the effective mass of the final  $e^+e^-$  pair (zero in the case of topology 2a);  
 $E_{c.m.s} = \sqrt{s}$ .

Equations:

$$f_1 = p_{t1} \sin \Theta_{t1} \cos \Phi_{t1} + p_{t2} \sin \Theta_{t2} \cos \Phi_{t2} + p_{ee} \sin \Theta_{ee} \cos \Phi_{ee} = 0 \quad (\text{A2.1})$$

$$f_2 = p_{t1} \sin \Theta_{t1} \sin \Phi_{t1} + p_{t2} \sin \Theta_{t2} \sin \Phi_{t2} + p_{ee} \sin \Theta_{ee} \sin \Phi_{ee} = 0 \quad (\text{A2.2})$$

$$f_3 = p_{t1} \cos \Theta_{t1} + p_{t2} \cos \Theta_{t2} + p_{ee} \cos \Theta_{ee} = 0 \quad (\text{A2.3})$$

$$f_4 = \sqrt{p_{t1}^2 - \mu^2} + \sqrt{p_{t2}^2 - \mu^2} + \sqrt{p_{ee}^2 + m_{ee}^2} - E_{c.m.s} = 0 \quad (\text{A2.4})$$

$$f_5 = \sqrt{p_{t1}^2 - \mu^2}/p_{t1} - n_1 \cos R_{t1} = 0 \quad (\text{A2.5})$$

$$f_6 = \sqrt{p_{t2}^2 - \mu^2}/p_{t2} - n_2 \cos R_{t2} = 0 \quad (\text{A2.6})$$

### Topology 3, mass fit only

Definitions:

$p_{t1}$  - measured tachyon candidate 1 track momentum;  
 $p_{t2}$  - measured tachyon candidate 2 track momentum;  
 $R_{t1}$  - measured radius of the anomalous ring associated with the tachyon candidate 1;  
 $R_{t2}$  - measured radius of the anomalous ring associated with the tachyon candidate 2;  
 $n_1$  and  $n_2$  - refraction indices of the radiators in which the corresponding rings were found;  
 $\mu$  - unknown (common) tachyon mass parameter;

Equations:

$$f_1 = \sqrt{p_{t1}^2 - \mu^2}/p_{t1} - n_1 \cos R_{t1} = 0 \quad (\text{A3.1})$$

$$f_2 = \sqrt{p_{t2}^2 - \mu^2}/p_{t2} - n_2 \cos R_{t2} = 0 \quad (\text{A3.2})$$

and a similar equation for each additional Cherenkov ring found.

## References

- [1] V. F. Perepelitsa, T. Ekelof, A. Ferrer, B. R. French, *A search for anomalous Cherenkov rings*, arXiv:hep-ex/1912.11839 (2019)
- [2] O. M .P. Bilaniuk, V. K. Deshpande, E. C. G. Sudarshan, “*Meta*”-relativity, Amer. J. Phys. **30** (1962) 718-723.
- [3] G. Feinberg, *Possibility of faster-than-light particles*, Phys.Rev. **159** (1967) 1089-1105.
- [4] E. P. Wigner, *Invariant quantum mechanical equations of motion*, in a book *Theoretical Physics*, pp. 59-82, I.A.E.A., Vienna, (1963)
- [5] Particle Data Group, Tanabashi et al., Phys. Rev. D **98**, No. 3, p. 414 (2018).
- [6] R. Sigal, A. Shamaly, *Tachyon behavior in general relativity*, Phys. Rev. D **10**, 2358-2361 (1974).
- [7] V. P. Perepelitsa, *Tachyon Michelson experiment*, Phys. Lett. B **67**, 471-473 (1977).
- [8] V. F. Perepelitsa, *Causality, Relativity and Faster-Than-Light Signals*, in a book *Philosophical Problems of the Hypothesis of Superluminal Velocities* (Nauka Press, Moscow, 1986), p. 40
- [9] J. Rembieliński, *Tachyons and preferred frames*, Int. J. Mod. Phys. A **12** (1997) 1677-1710.
- [10] M. J. Radzikowski, *Stable, renormalizable, scalar tachyonic quantum field theory with chronology protection*, arXiv:math-ph/0804.4534 (2008).
- [11] V. F. Perepelitsa, *Looking for a theory of faster-than-light particles*, arXiv:gen-ph/1407.3245 (2014).
- [12] V. F. Perepelitsa, *How to implant a causal Theta-function into a tachyon field operator, or why tachyons do not violate causality* , arXiv:gen-ph/1512.07921 (2015).
- [13] DELPHI Collaboration, P. Aarnio et al., Nucl. Instr. and Meth. A **303** (1991) 233.
- [14] DELPHI Collaboration, P. Abreu et al., Nucl. Instr. and Meth. A **378** (1996) 57.
- [15] W. Adam et al., Nucl. Instr. and Meth. A **343** (1994) 68.
- [16] W. Adam et al., Nucl. Instr. and Meth. A **360** (1995) 416.
- [17] W. Adam et al., Nucl. Instr. and Meth. A **367** (1995) 233.
- [18] W. Adam et al., Nucl. Instr. and Meth. A **371** (1996) 12.

- [19] E. Albrecht et al., Nucl. Instr. and Meth. A **433** (1999) 47.
- [20] M. Battaglia, P. M. Kluit, DELPHI note, DELPHI 96-133 RICH 90, <http://inspirehep.net/record/1659476>
- [21] V. F. Perepelitsa, *Experimental aspects of the tachyon hypothesis*, arXiv:gr-qc/1606.04808 (2016)
- [22] ALICE Collaboration, B. Abelev et al., Int. J. Mod. Phys A **29**, 1430044 (2014)
- [23] LHCb Collaboration, A. A. Alves Jr. et al., J. Instrum. **3**, (2008) S08005.
- [24] LHCb RICH Collaboration, M. Adinoli et al., Eur. Phys. J. C **73** (2015) 2431.

**Table 1.** Some input and output parameters of the kinematic fit of events of topology 1.

Run Event	Beam	$p_1$ meas $p_2$ meas	$p_1$ fit $p_2$ fit	$\mu$ , error	$E_\gamma^{ISR}$ , error	fit $\chi^2$ , ndf	$r_1$ meas $r_2$ meas (mrad)	$r_1$ fit $r_2$ fit (mrad)	$dE/dx$ , meas (mip)	$dE/dx$ , fit (mip)
71768 6277	86.2	$92 \pm 19$ Not meas.	73.8 12.9	4.29 $\pm 0.31$		5.0 6	$85 \pm 3$ $347 \pm 15$ $741^* \pm 19$	85 347 737*	3.28 $\pm 0.12$	3.00
84451 478	94.6	$64 \pm 4$ $10 \pm 1$	67.9 11.1	4.98 $\pm 0.27$	19.9 $\pm 3.9$	13.7 6	$102 \pm 5$ $460 \pm 16$ $786^* \pm 20$	96 470 793*	Not meas.	2.86
86748 757	94.6	$13 \pm 1$ $87 \pm 10$	12.9 82.1	4.19 $\pm 0.28$		2.0 6	$335 \pm 14$ $79 \pm 3$ $747^* \pm 19$	337 80 733*	Not meas.	3.02
101830 15719	96.1	$54 \pm 5$ Not meas.	65.1 31.1	2.75 $\pm 0.27$		5.1 5	$75 \pm 3$ $107 \pm 4$	75 108	3.14 $\pm 0.10$	3.17
102500 9258	96.1	$59 \pm 7$ Not meas.	78.4 6.4	4.65 $\pm 0.39$	16.6 $\pm 3.1$	17.5 5	$85 \pm 3$ $1010^* \pm 27$ $816 \pm 34$	86 $1002^*$ 817	2.50 $\pm 0.10$	2.34
106061 3293	100.1	$94 \pm 9$ $7.6 \pm 1$	93.8 7.7	5.96 $\pm 0.36$		3.1 5	$91 \pm 4$ $885 \pm 35$ $1052^* \pm 23$	89 894 $1055^*$	Not meas.	2.22
107038 11748	100.1	$74 \pm 7$ Not meas.	90.8 10.2	5.49 $\pm 0.41$		6.6 5	$87 \pm 4$ $583 \pm 22$	87 574	3.04 $\pm 0.11$	2.72
116892 5928a	103.0	Not meas. $21 \pm 2$	85.0 19.3	4.89 $\pm 0.29$		4.4 7	$83 \pm 3$ $266 \pm 12$ $702^* \pm 17$	85 263 707*	2.87 $\pm 0.17$	3.08
116892 5928b	103.0	$140 \pm 24$ Not meas.	98.8 5.6	4.14 $\pm 0.50$		4.4 7	$75 \pm 2$ $1021^* \pm 27$ $831 \pm 30$	75 $1015^*$ 837	Not meas.	2.31

\* Asterisks designate liquid radiator rings.

Remarks to Table 1 (valid also for subsequent tables):

- 1). Beam and tachyon momenta  $p_1, p_2$  in tables are given in GeV/ $c$ , tachyon mass parameters are given in GeV/ $c^2$ , the ISR photon energies are given in GeV.
- 2). If the ISR photon energy is absent in the corresponding column, this means that it was calculated to be below 1.5 GeV and it is dropped from the fit.
- 3). If 3rd (4th) anomalous ring was found in a given event, its parameters are quoted in the 3rd (4th) line of the event raw.
- 4). The number of constraint equations equals to 4 plus the number of the anomalous rings found. In events with the (common) track ionization measured an additional constraint, based on the ionization, is added.
- 5). The number of unknowns equals to 1 (tachyon mass parameter common for both tachyons) plus number of unmeasured tachyon momenta (1 in most of the events of topology 1) plus 1 if an ISR photon momentum (energy) participates in the fit.

**Table 2.** Some input and output parameters of the kinematic fit of events of topology 2.

Run Event	Beam	$p_1$ meas $p_2$ meas	$p_1$ fit $p_2$ fit	$\mu$ , error	Final $e^+e^-$ longitudinal $\Delta p$ , error	Mass of $e^+e^-$	fit $\chi^2$ , ndf	$r_1$ meas $r_2$ meas (mrad)	$r_1$ fit $r_2$ fit (mrad)
77190 2950	91.6	$5.1 \pm 0.1$ $4.7 \pm 0.3$	5.03 5.20	0.296 $\pm 0.019$	1.2 $\pm 0.1$	173.0 $\pm 0.2$	5.3 3	$84 \pm 3$ $86 \pm 4$	86 84
85371 626	94.6	$9.6 \pm 0.2$ $9.6 \pm 0.2$	9.48 9.71	0.881 $\pm 0.039$	1.0 $\pm 0.1$	170.1 $\pm 0.3$	4.8 3	$118 \pm 5$ $104 \pm 4$	112 110
88975 84	94.6	$4.4 \pm 0.1$ $4.1 \pm 0.1$	4.41 4.09	0.155 $\pm 0.015$	1.1 $\pm 0.1$	180.7 $\pm 0.1$	0.4 3	$72 \pm 3$ $72 \pm 3$	71 73
105033 3999	100.1	$6.7 \pm 0.1$ $5.8 \pm 0.1$	6.61 5.97	0.284 $\pm 0.023$	1.4 $\pm 0.1$	187.6 $\pm 0.2$	7.3 3	$76 \pm 2$ $78 \pm 4$	74 78
110546 15356	102.5	$100.5 \pm 6.5$ $103.3 \pm 6.7$	102.4 102.5	4.30 $\pm 0.46$			4.7 5	$75 \pm 3$ $75 \pm 4$	75 75
115187 4860	103.0	$6.0 \pm 0.1$ $5.7 \pm 0.1$	5.95 5.82	0.268 $\pm 0.022$	1.6 $\pm 0.1$	194.2 $\pm 0.2$	7.2 3	$75 \pm 3$ $78 \pm 4$	77 77

**Table 3.** Some input and output parameters of the kinematic fit of events of topology 3.

Run Event	Beam	$p_e$ fit	$p_1$ meas $p_2$ meas	$p_1$ fit $p_2$ fit	$\mu$ , error	fit $\chi^2$ , ndf	$r_1$ meas $r_2$ meas (mrad)	$r_1$ fit $r_2$ fit (mrad)
41633 1568	46.5	46.5	$12.03 \pm 1.51$ $4.72 \pm 0.69$	9.62 4.70	0.302 $\pm 0.039$	7.9 6	$72 \pm 3$ $89 \pm 5$	70 89
42495 24853	45.6	45.6	$21.28 \pm 2.61$ $8.89 \pm 0.71$	15.83 8.78	0.781 $\pm 0.073$	6.0 3	$82 \pm 4$ $107 \pm 5$	79 109
46877 4278	45.6	$\approx 41.7$	$6.46 \pm 0.31$ $28.99 \pm 0.76$	6.43 28.70	4.71 $\pm 0.13$	1.1 2	$815 \pm 32$ $181 \pm 7$ $987^* \pm 26$	826 176 1008*
49062 2354	45.6	$\approx 30.4$	$19.69 \pm 4.02$ $3.79 \pm 0.12$	16.33 4.25	0.896 $\pm 0.137$	1.2 1	$84 \pm 4$ $220 \pm 10$	83 221
49316 584	45.6	$\approx 31.1$	$18.00 \pm 3.30$ $5.67 \pm 0.47$	20.27 5.49	0.933 $\pm 0.082$	0.9 1	$76 \pm 4$ $183 \pm 9$	77 182
50971 4331	45.6	$\approx 37.6$	$8.83 \pm 0.89$ $4.46 \pm 1.02$	8.67 4.87	0.297 $\pm 0.040$	0.3 1	$72 \pm 4$ $86 \pm 5$	71 87
58547 23906	45.6	45.7	$12.17 \pm 1.30$ $10.90 \pm 1.22$	13.11 12.56	0.993 $\pm 0.073$	3.8 3	$99 \pm 5$ $99 \pm 5$	98 101
62192 20534	46.5	$\approx 39.3$	$15.45 \pm 2.95$ $7.17 \pm 0.17$	12.43 7.19	4.57 $\pm 0.18$	1.7 3	$380 \pm 16$ $695 \pm 29$ $930^{**} \pm 28$ $1024^{**} \pm 31$	381 691 940** 1059**
79940 2890	91.6	79.5	$99.6 \pm 36.8$ $5.36 \pm 1.65$	72.31 7.35	3.96 $\pm 0.40$	1.2 3	$83 \pm 3$ $580 \pm 24$ $832^* \pm 21$ $990^{**} \pm 30$	83 571 847* 1007**

**Table 3, Continued.** Some input and output parameters of the kinematic fit of events of topology 3.

Run Event	Beam	$p_e$ fit	$p_1$ meas $p_2$ meas	$p_1$ fit $p_2$ fit	$\mu$ , error	fit $\chi^2$ , ndf	$r_1$ meas $r_2$ meas (mrad)	$r_1$ fit $r_2$ fit (mrad)
104949 27827	100.1	100.1	$11.94 \pm 1.24$ $7.35 \pm 1.89$	11.02 6.79	4.64 $\pm 0.49$	4.2 7	$442 \pm 17$ $742 \pm 31$ $792^* \pm 21$ $978^* \pm 26$	439 756 778* 961*
105892 13127	100.1	100.1	$3.67 \pm 0.60$ $3.30 \pm 0.23$	3.50 3.48	0.290 $\pm 0.033$	1.6 5	$104 \pm 4$ $104 \pm 4$	104 104

\* Asterisks designate the liquid radiator rings.

\*\* Double asterisks designate the quartz radiator rings.

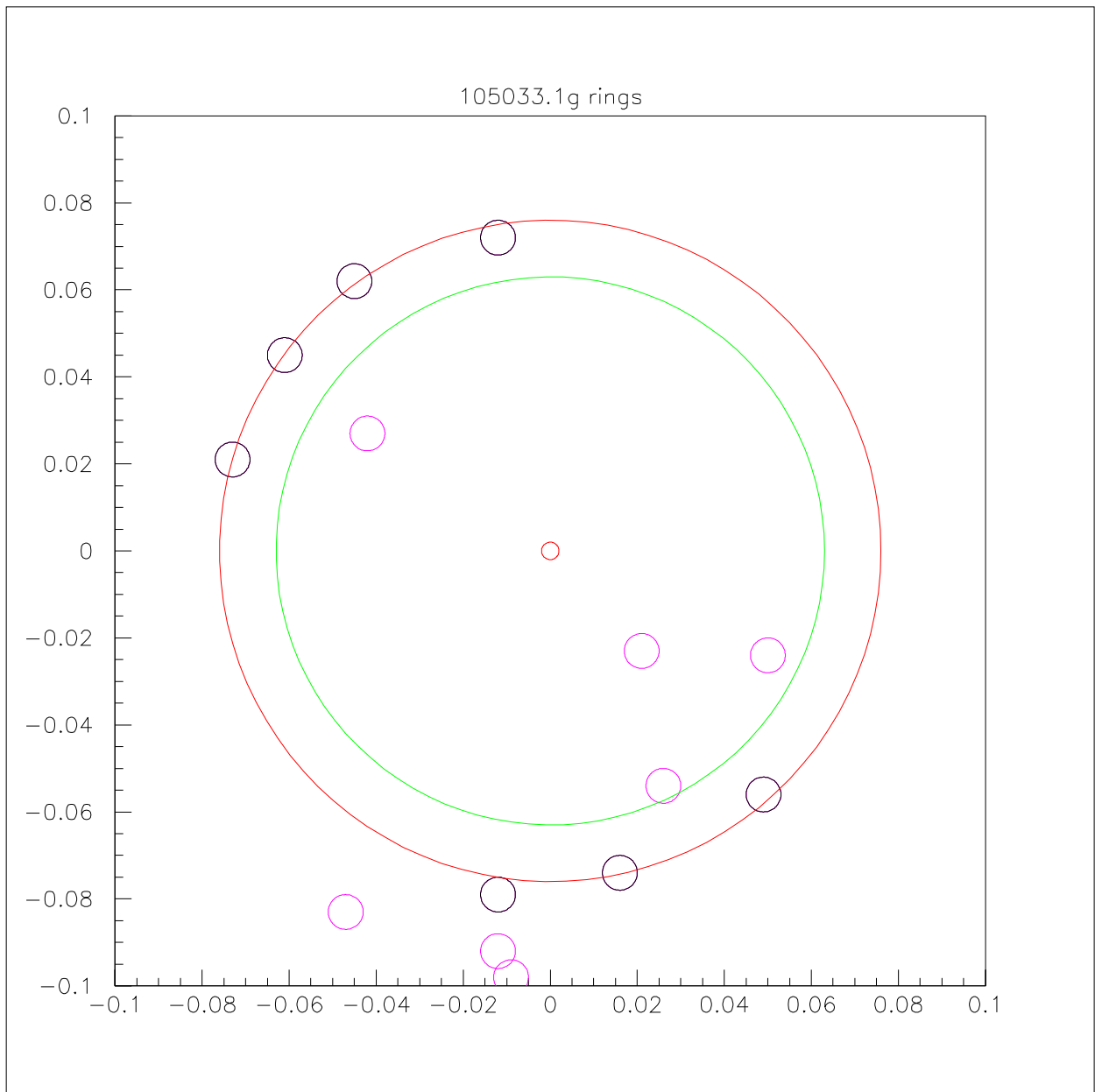


Figure 1: Gas radiator hit pattern for the 1st track of the event of topology 2b 105033:3999 and a ring of a radius 76 mrad produced by the track. Small circles in the hit pattern represent the RICH hits; their radii are equal to single photon angular accuracy  $\sigma$  in the vicinity of the ring under consideration. The hits pertaining to the anomalous ring are plotted in bold. The (inner) green circle marks the position and the size of a standard ring (not seen in the pattern). The probability of anomalous ring (marked by the red circle) to be fortuitously reconstructed from background hits is below  $1.2 \times 10^{-4}$ . The small red circle in its center marks the origin of the Cherenkov plane, i.e. the position of the image of the track impact point,  $x = 0$ ,  $y = 0$ . The axes in this figure, as well as in all analogous ones below, represent coordinates of individual hits on the Cherenkov plane; the axes scale values are given in radians.

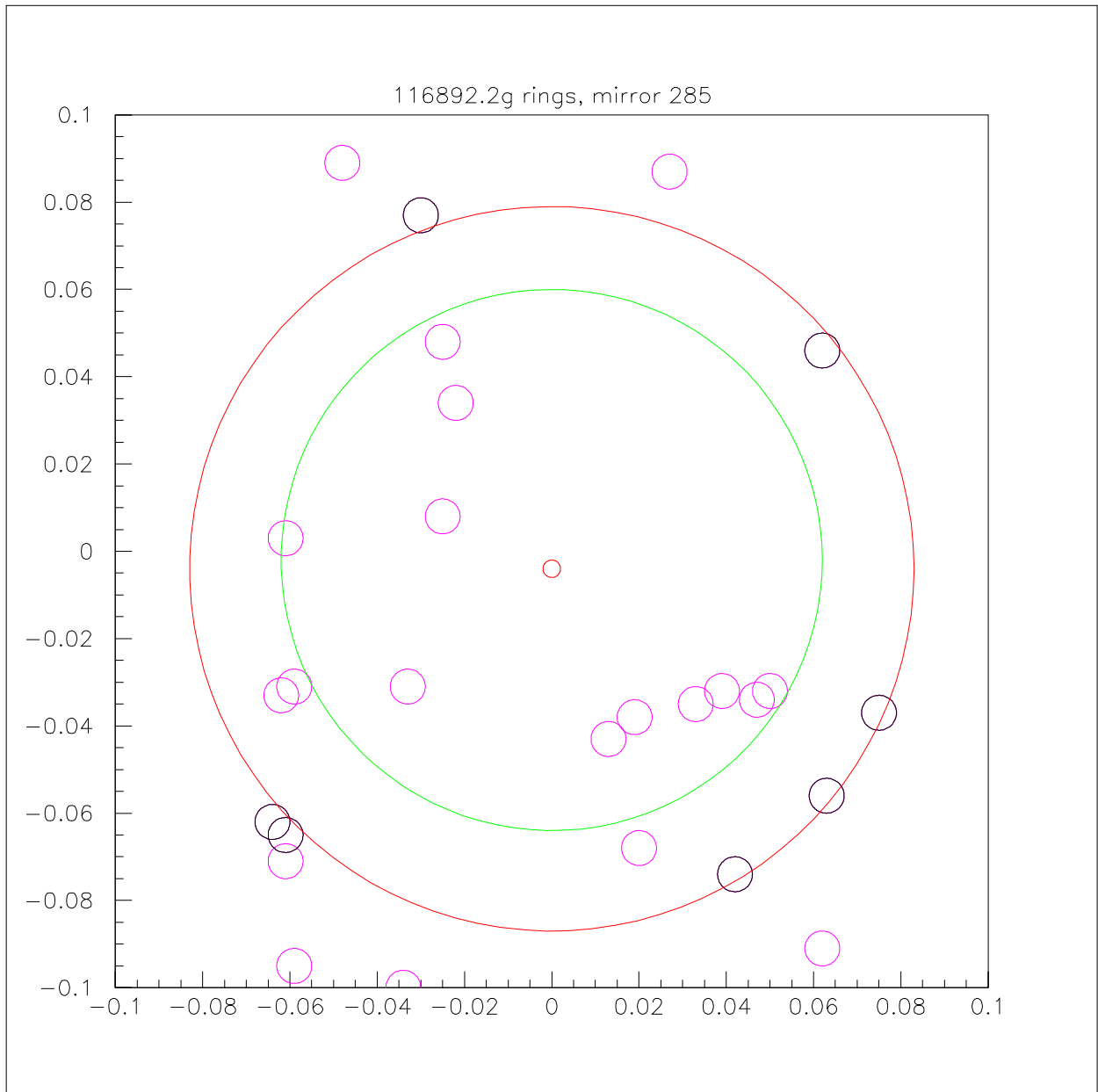


Figure 2: Gas radiator hit pattern for a track of the event of topology 1a 116892:5928a, and a ring of a radius 83 mrad produced by the track. The green circle marks the position and the size of a standard ring (not seen in the pattern). The probability of anomalous ring (marked by the red circle) to be fortuitously reconstructed from background hits is below  $9.0 \times 10^{-3}$ . The units in the Cherenkov plane are given in radians, the small red circle in its center marks the position of the image of the track impact point.

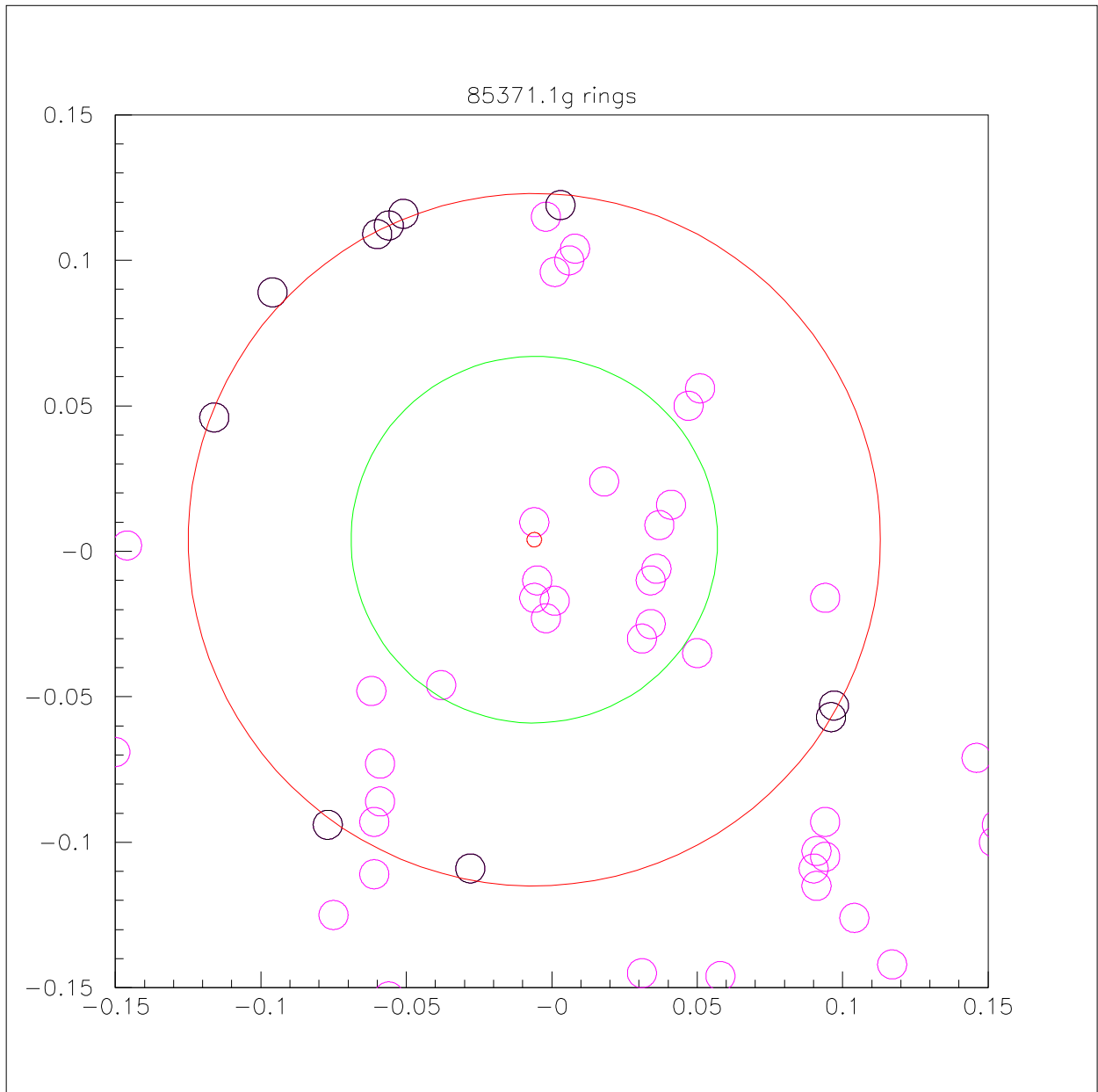


Figure 3: Gas radiator hit pattern for the 1st track of the event of topology 2b 85371:626, and a ring of a radius 118 mrad produced by the track. The green circle marks the position and the size of a standard ring (not seen in the pattern). The probability of anomalous ring (marked by the red circle) to be fortuitously reconstructed from background hits is below 0.0158. The units in the Cherenkov plane are given in radians, the small red circle in its center marks the position of the image of the track impact point.

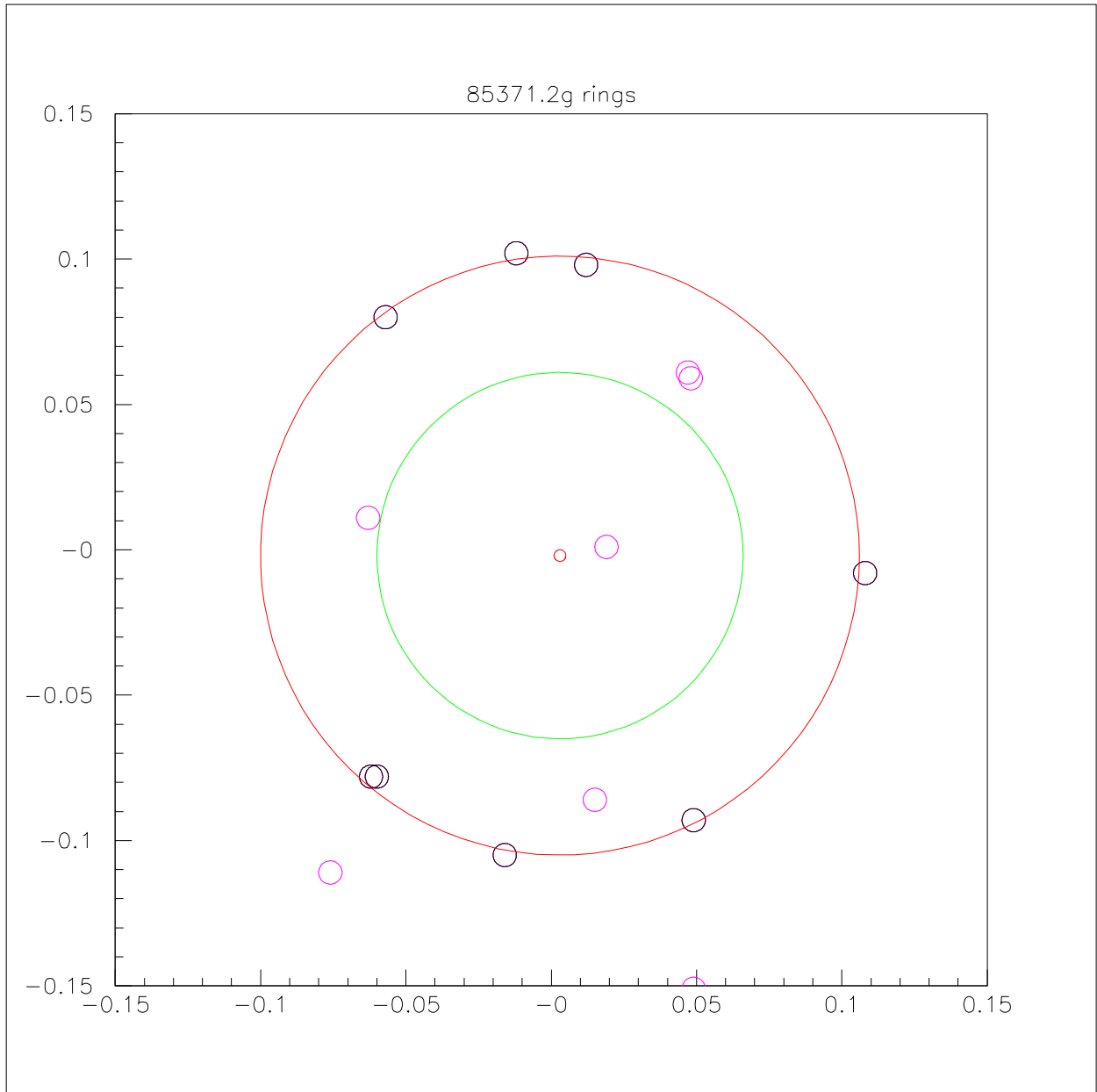


Figure 4: Gas radiator hit pattern for the 2nd track of the event 85371:626 (the same event as presented by another ring in the previous figure, Fig. 3), and a ring of a radius 104 mrad produced by this track. The green circle marks the position and the size of a standard ring (not seen in the pattern). The probability of anomalous ring (marked by the red circle) to be fortuitously reconstructed from background hits is below  $6.4 \times 10^{-5}$ . The units in the Cherenkov plane are given in radians, the small red circle in its center marks the position of the image of the track impact point.

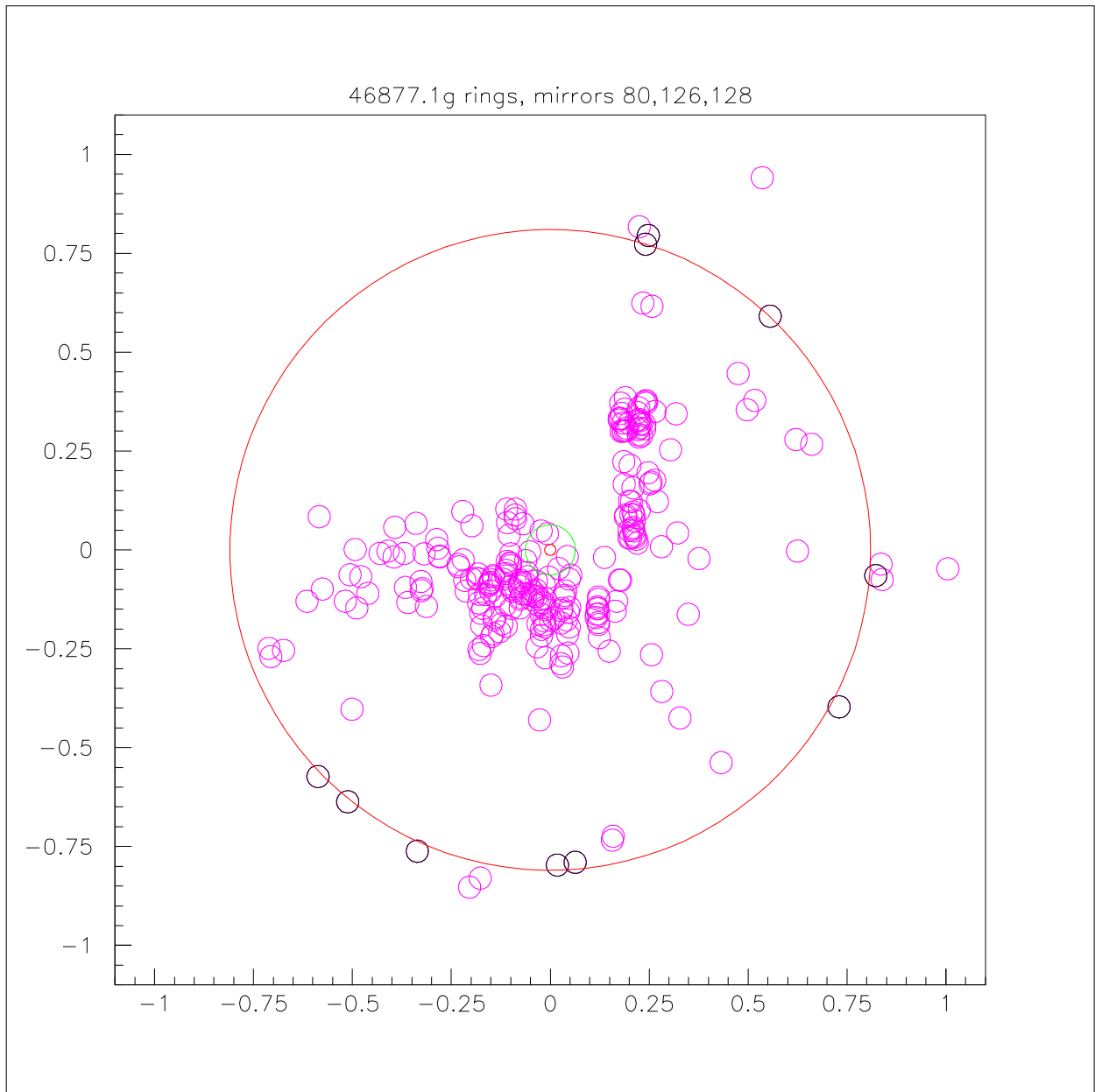


Figure 5: Gas radiator hit pattern for one of the tracks in a 3-particle jet of an event of topology 3 46877:4278, and a ring of a radius 815 mrad produced by this track. The green circle in the center of the hit pattern marks the position and the size of a standard ring (not seen in the pattern). The probability of anomalous ring (marked by the red circle) to be fortuitously reconstructed from background hits is below  $1.7 \times 10^{-4}$ . The units in the Cherenkov plane are given in radians, the small red circle in its center marks the position of the image of the track impact point.

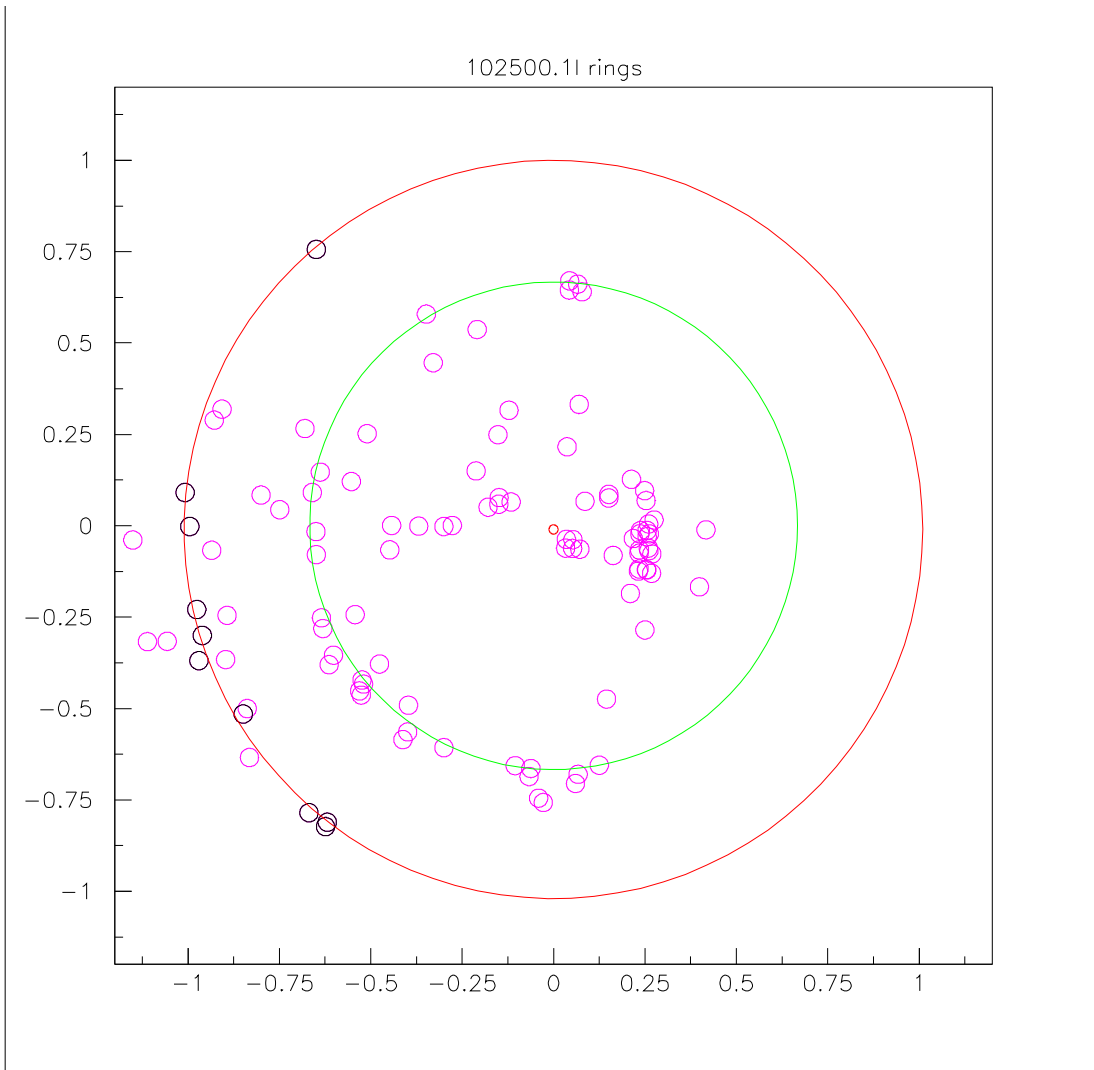


Figure 6: Liquid radiator hit pattern for a double track of an event of topology 1a 102500:9258. Together with an anomalous ring (indeed, an arc due to the effect of the total inner reflection), having radius of 1010 mrad and marked by a red circle, a ring of a radius of 674 mrad (close to the radius of a standard ring 667 mrad and also presented as an arc) marked by a green circle, is seen. The probability of the anomalous ring to be fortuitously reconstructed from background hits is below  $2.4 \times 10^{-3}$ .

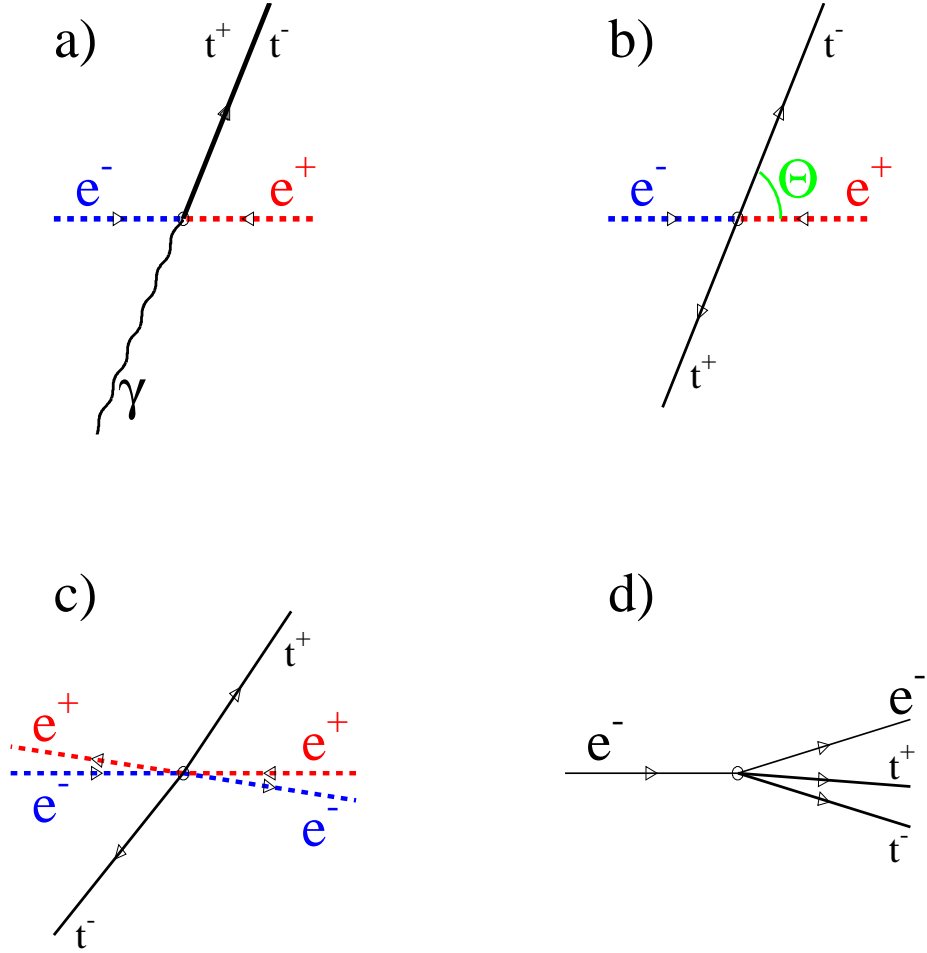


Figure 7: Reaction diagrams of topologies studied: **a)** topology 1, production of a tachyon-antitachyon pair with nearly-zero opening angle; **b)** topology 2a, back-to-back tachyon-antitachyon production; **c)** topology 2b generated by a different mechanism of the tachyon-antitachyon pair production, via a  $\gamma \gamma$  interaction; **d)** topology 3, electroproduction of a tachyon-antitachyon pair on nuclei in the detector material. The dashed lines mark beam particles and/or the particles that go undetected escaping into the beam pipe.

 <b>DELPHI</b> Run: 107038 Evt: 11748 Beam: 100.1 GeV Proc: 19-Mar-2019 DAS: 21-Oct-1999 Scan: 27-May-2019 06:48:54 Tan+DST	TD	TE	TS	TK	TV	ST	PA
	54	42	0	1	0	0	0
	( 54 Y 42 Y 0 X 1 Y 0 Y 0 Y 0 )						
	Deact	0	0	0	0	0	0
	( 0 Y 0 Y 0 Y 0 Y 0 Y 0 Y 0 )						

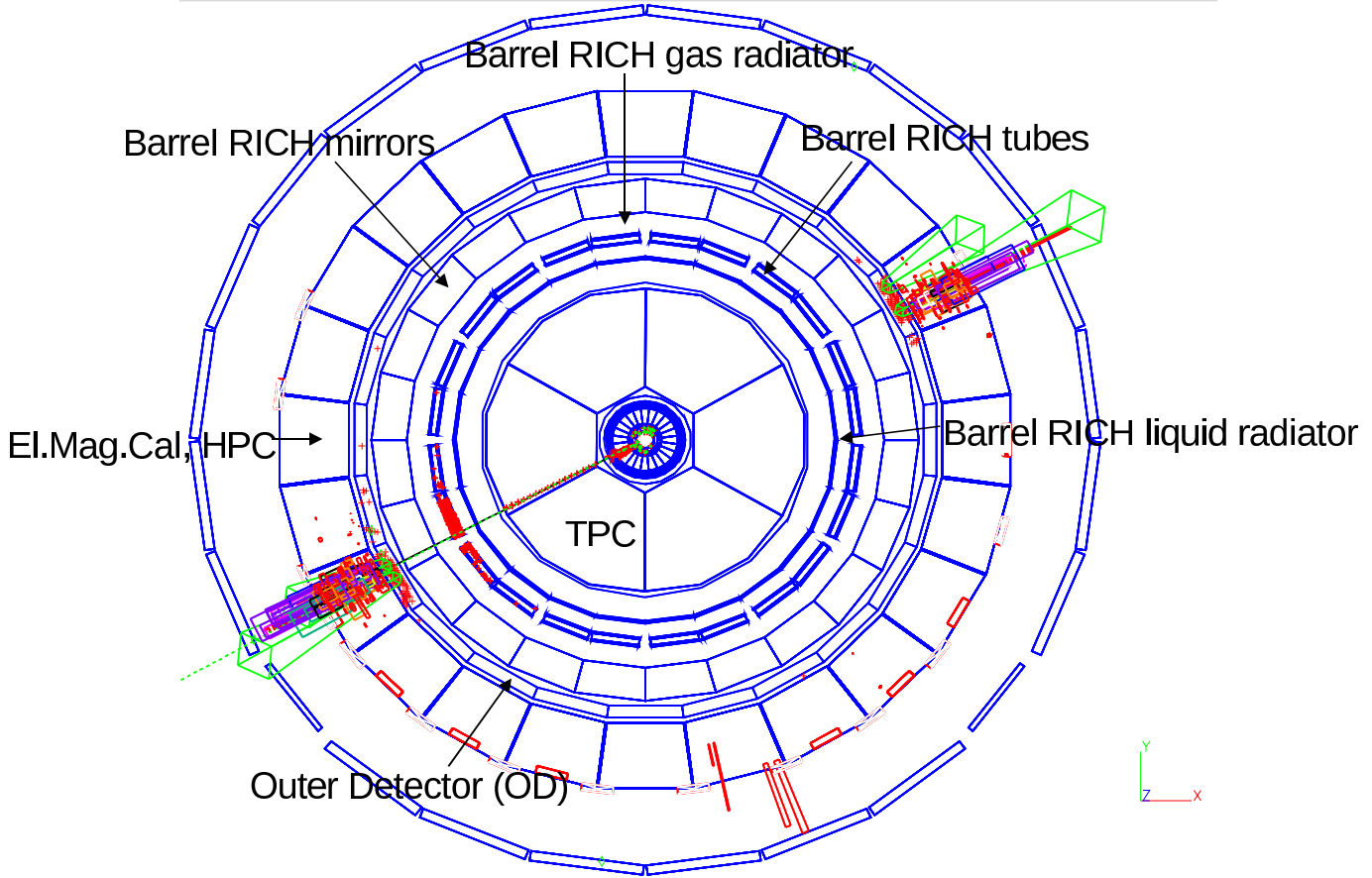


Figure 8: An example of event of topology 1a of reaction (3.1) with two tracks non-resolved in the TPC, a general view. The red hits inside the Barrel RICH drift tubes are Barrel RICH hits (the tubes will not be shown in next figures).

	<b>DELPHI</b>	<b>Run: 107038</b>	<b>Evt: 11748</b>						
		<b>Beam: 100.1 GeV</b>	<b>Proc: 19-Mar-2019</b>						
		<b>DAS: 21-Oct-1999</b>	<b>Scan: 27-May-2019</b>						
		<b>06:48:54</b>	<b>Tan+DST</b>						

	TD	TE	TS	TK	TV	ST	PA
Act	54	41	0	1	0	0	0
	( 54 Y	42 Y	0 )	( 1 Y	0 Y	0 Y	0 )
Deact	0	0	0	0	0	0	0
	( 0 X	0 X	0 X	0 X	0 X	0 X	0 )

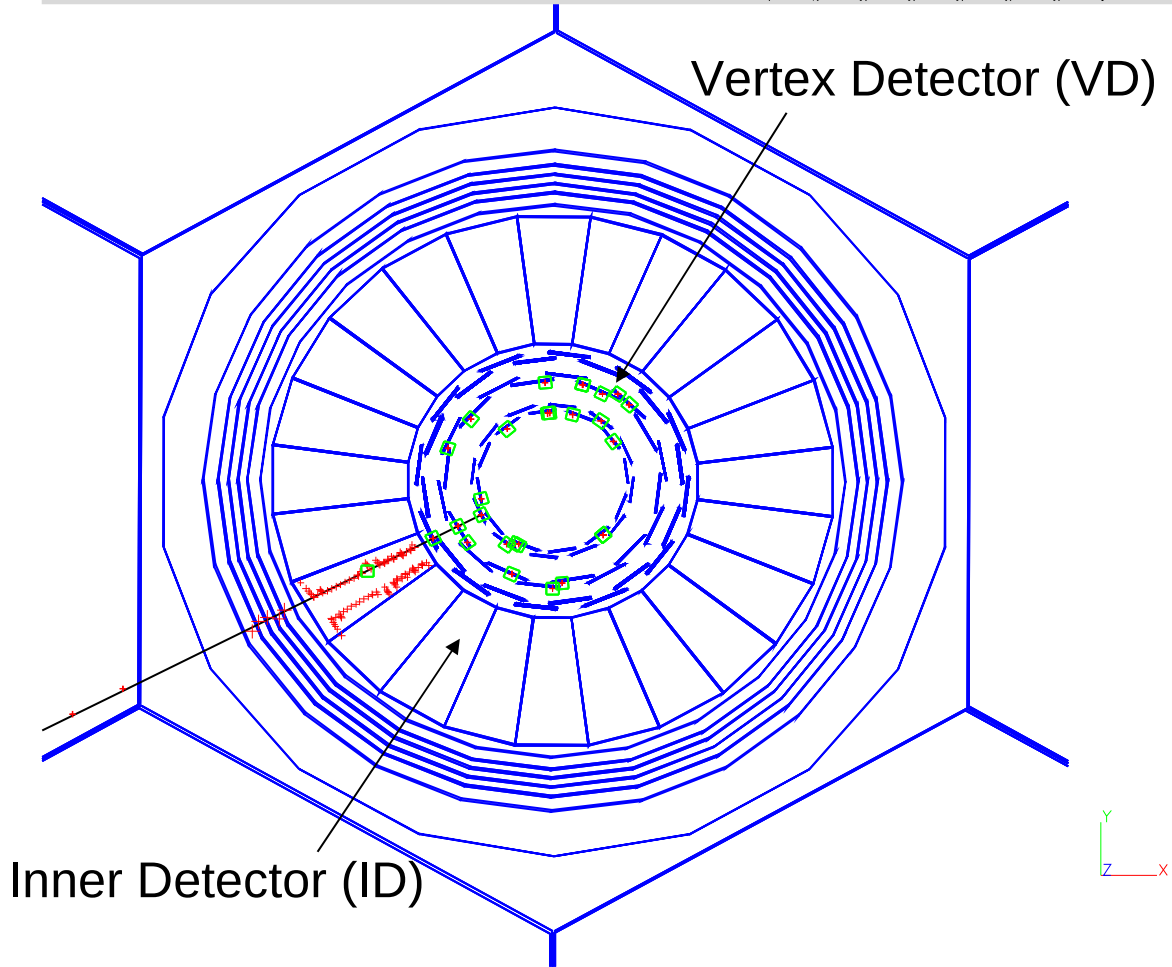


Figure 9: The same event, the central detector (VD and ID) view.

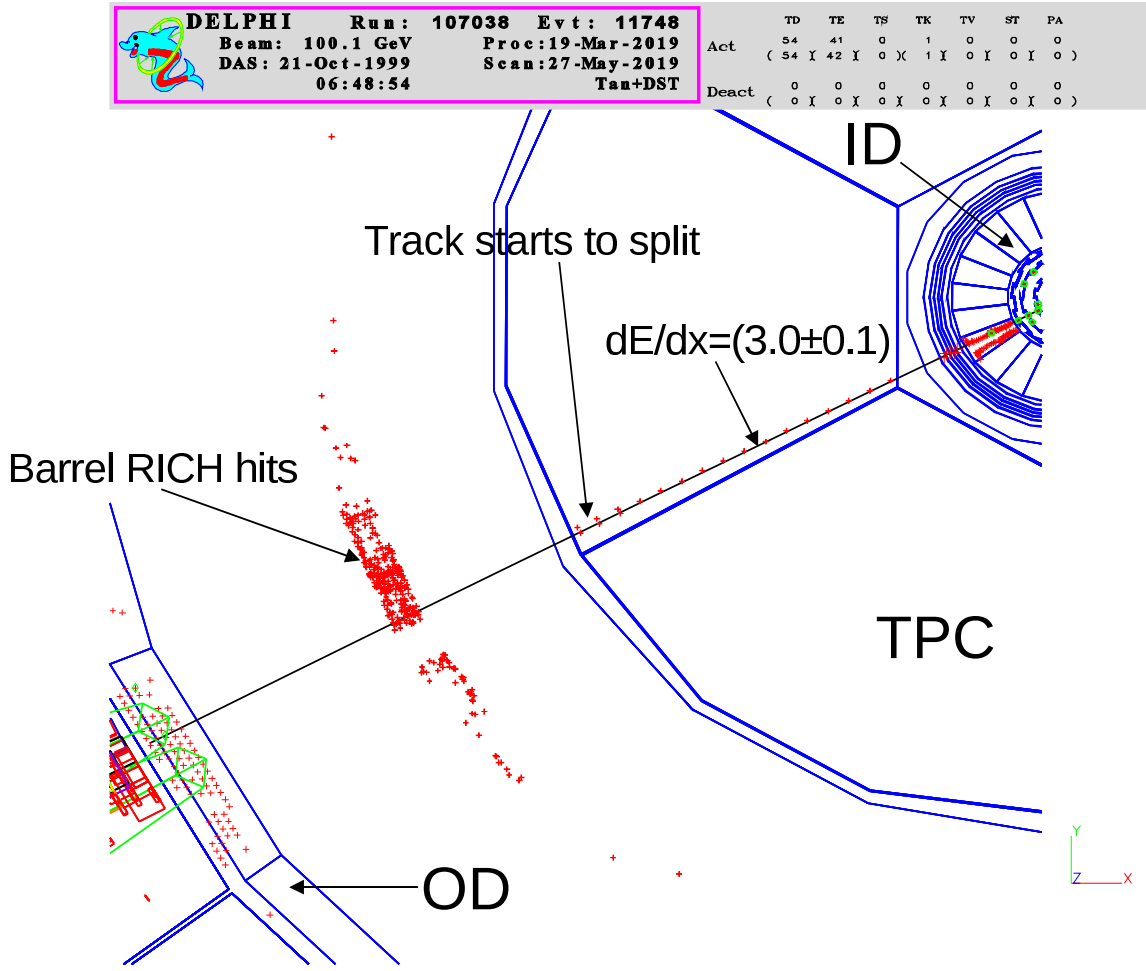


Figure 10: The same event, the TPC view showing the non-resolved track starting to split. The  $dE/dx$  units are mips (see footnote 7 on page 6).

	<b>DELPHI</b>	<b>Run :</b>	<b>86748</b>	<b>Evt :</b>	<b>757</b>														
		<b>Beam:</b>	94.6 GeV	<b>Proc:</b>	24-Feb-2014	Act	109	104	0	0	0	0							
		<b>DAS:</b>	17-Aug-1998	<b>Scan:</b>	8-Mar-2014		(109)	(105)	X	0	X	4	X	0	X	0	X	0	)
			01:04:28		<b>Tan+DST</b>	Deact	0	0	0	0	0	0	0	0	0	0	0	0	)

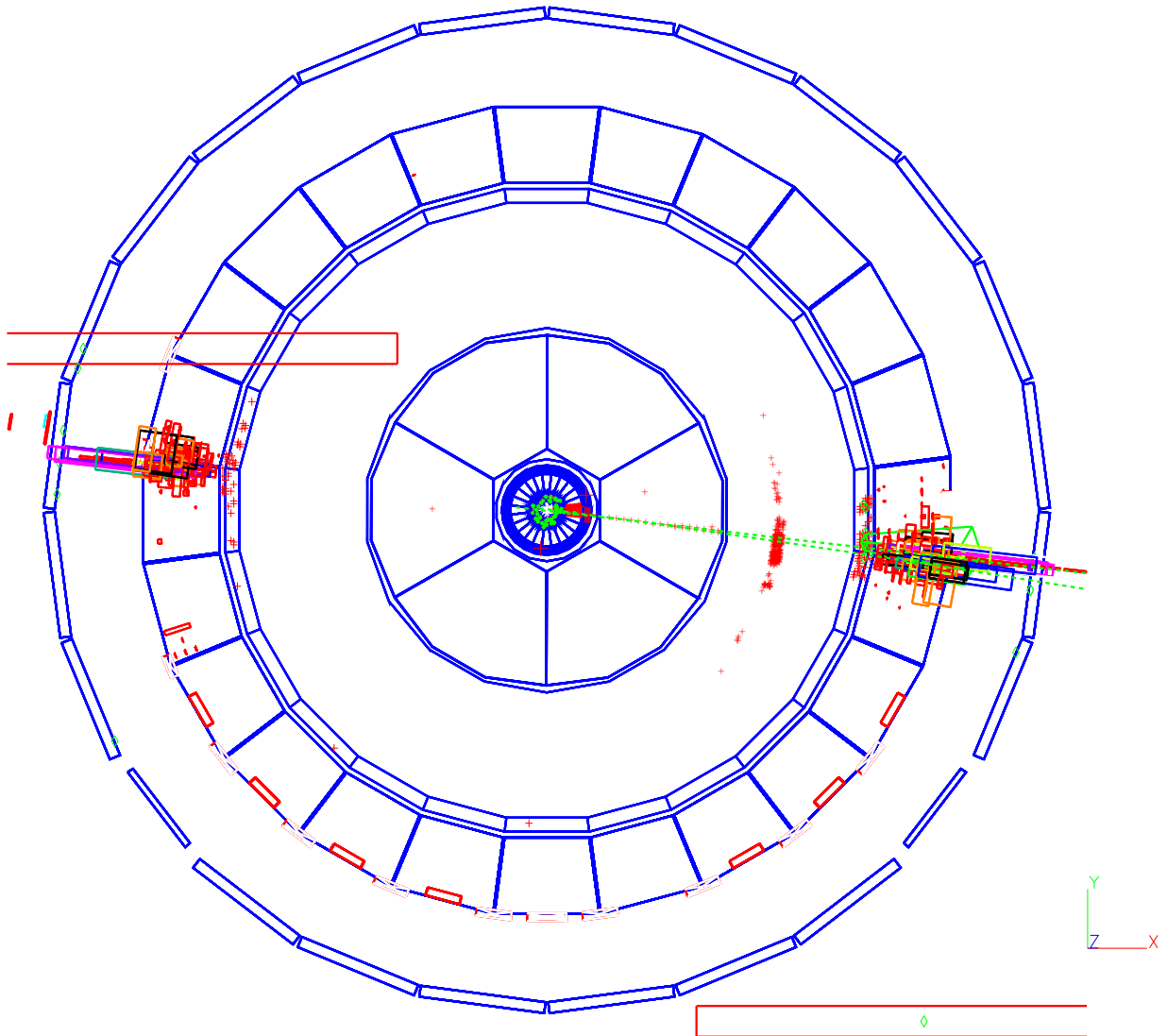


Figure 11: An example of event of topology 1b of reaction (3.1) with two tracks resolved in the TPC, a general view.

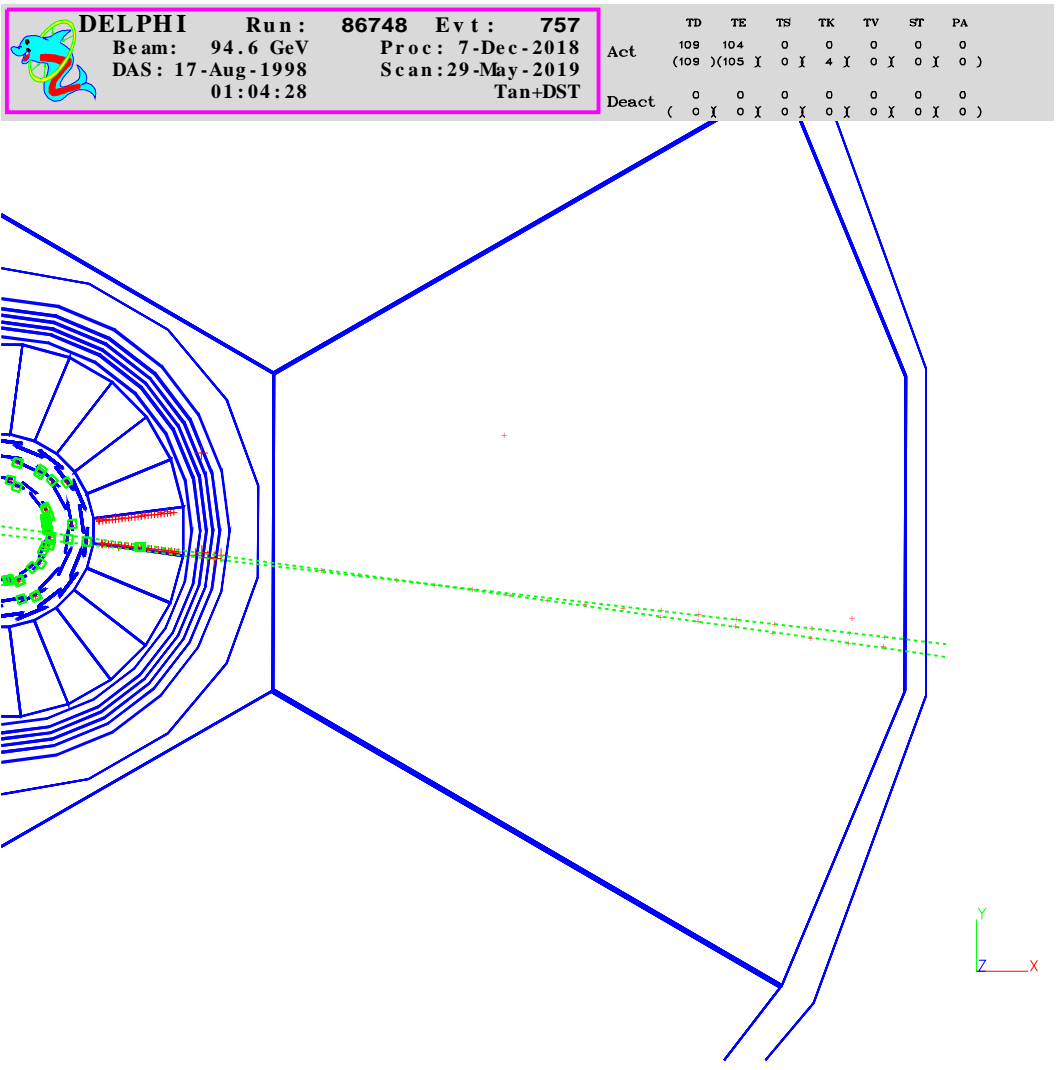


Figure 12: The same event, the VD, ID and TPC view of the two-particle resolved jet.

 <b>DELPHI</b>	<b>Run: 110546</b>	<b>Evt: 15356</b>
	<b>Beam: 103.0 GeV</b>	<b>Proc: 7-Mar-2019</b>
	<b>DAS: 28-May-2000</b>	<b>Scan: 27-May-2019</b>
	<b>21:55:47</b>	<b>Tan+DST</b>

	TD	TE	TS	TK	TV	ST	PA
Act	61	48	0	2	0	0	0
	( 61 Y	49 Y	0 Y	3 Y	0 Y	0 Y	0 )
Deact	0	0	0	0	0	0	0
	( 0 Y	0 Y	0 Y	0 Y	0 Y	0 Y	0 )

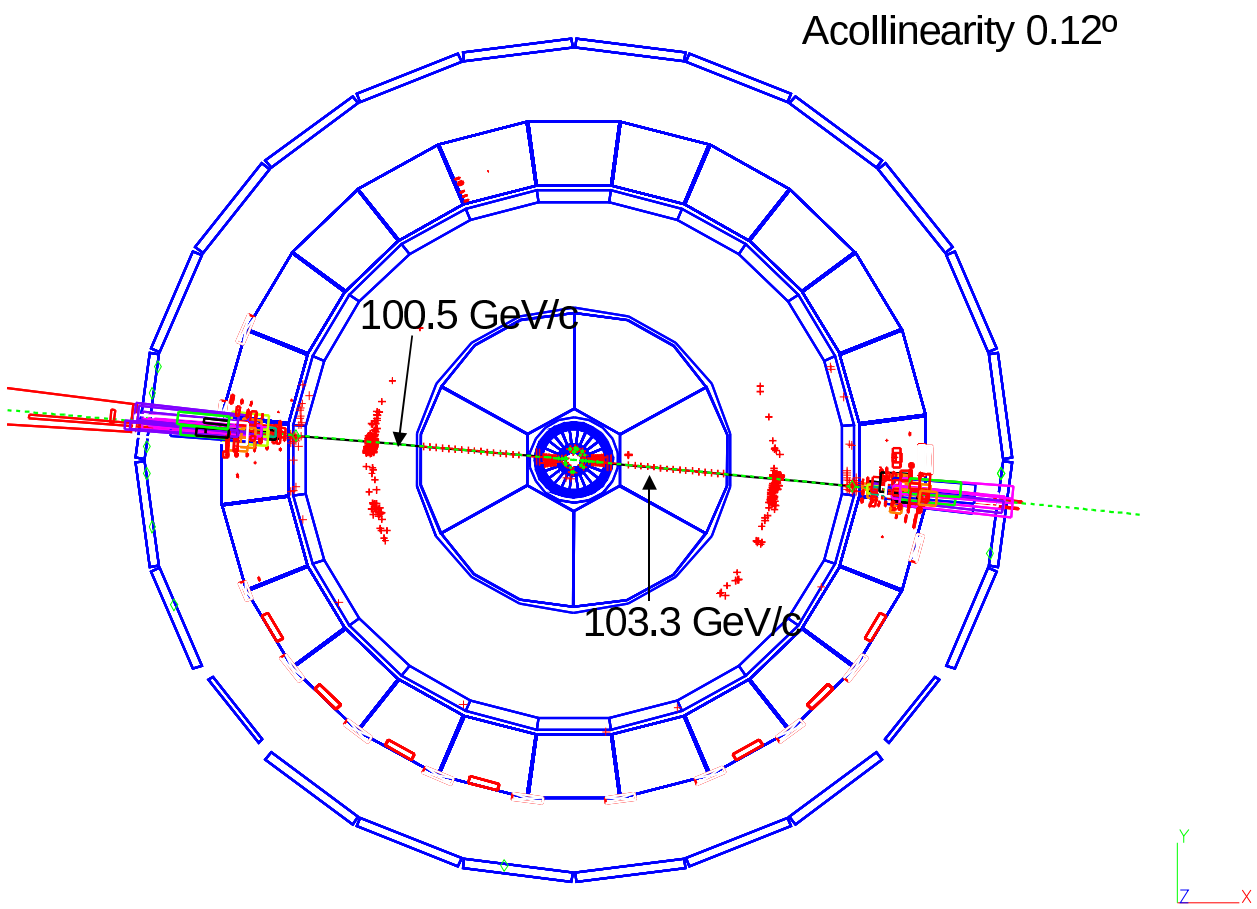


Figure 13: An example of event of topology 2a of reaction 3.2, a general view.



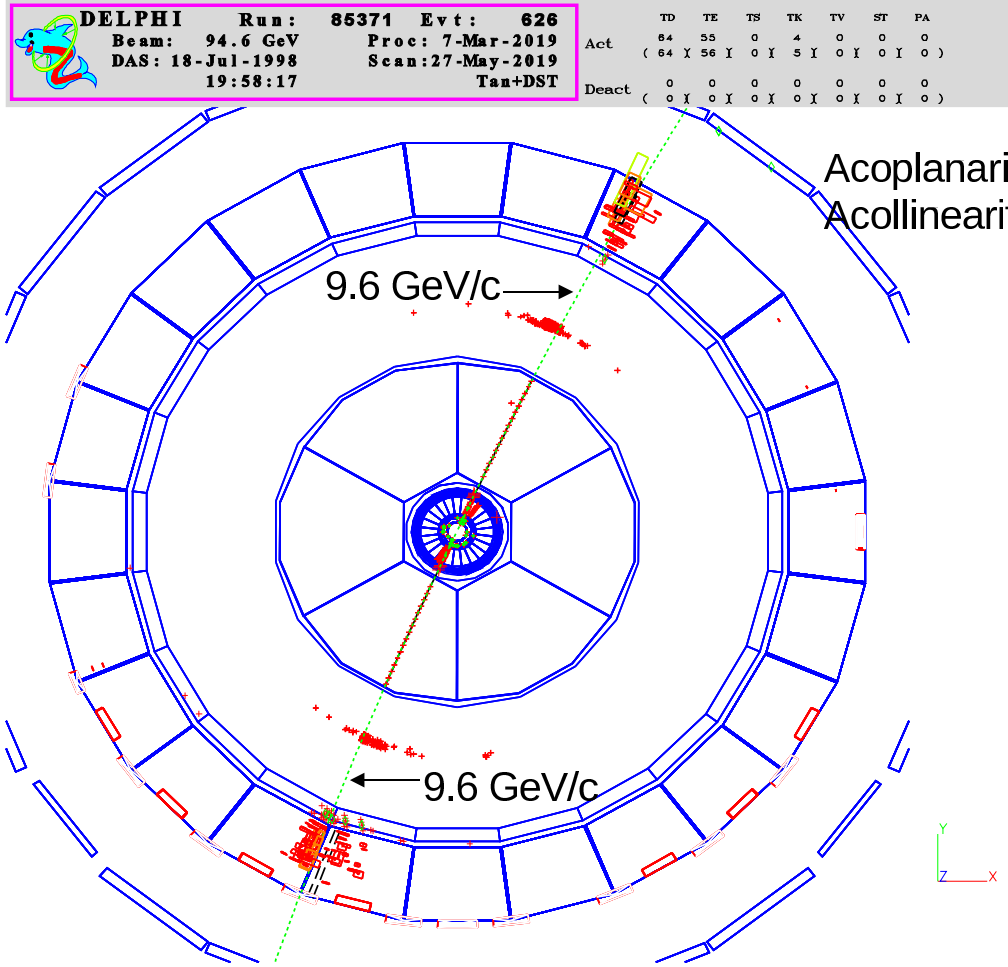


Figure 15: An example of event of topology 2b of reaction 3.3, a general view.

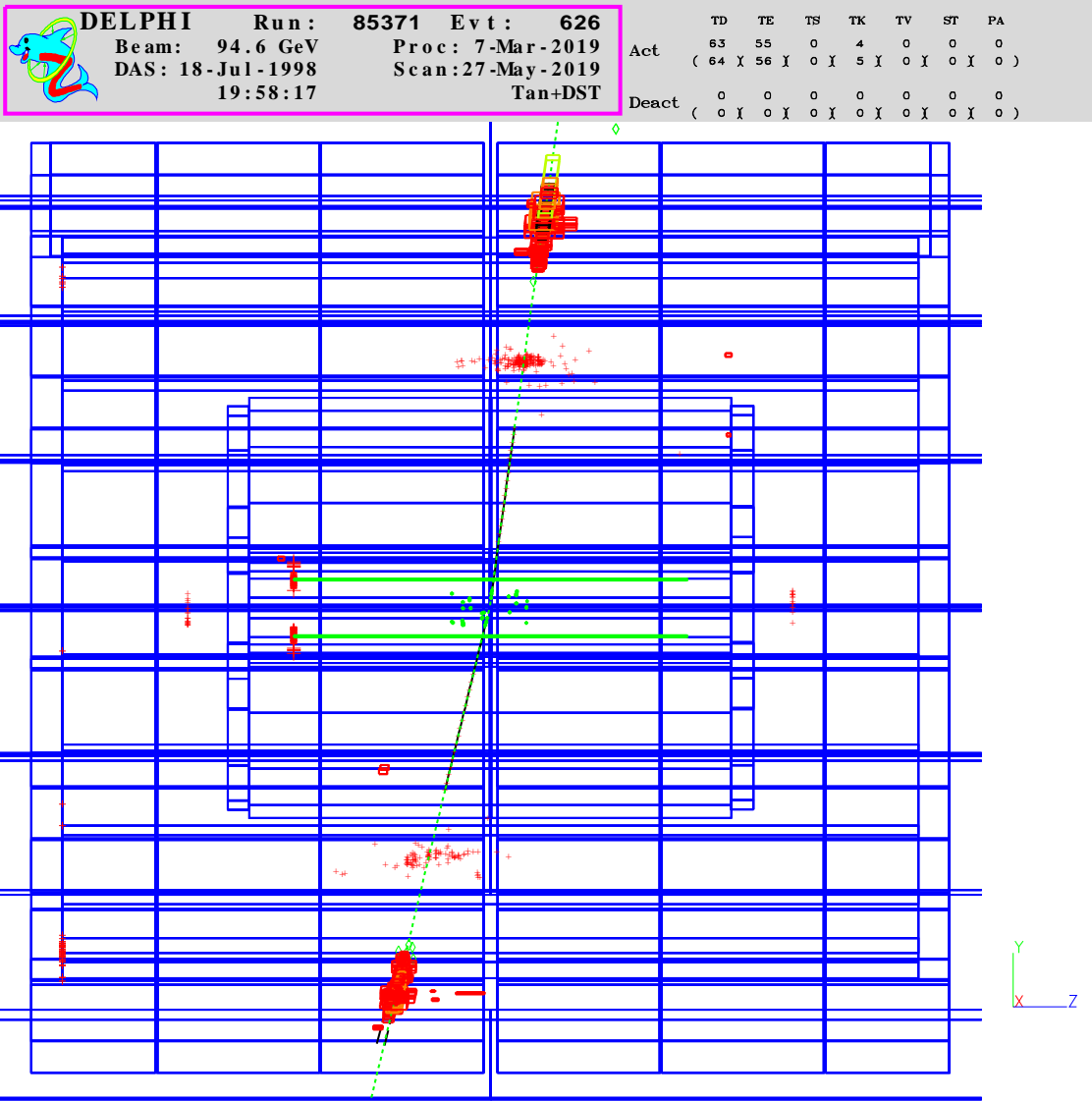


Figure 16: The same event, the YZ view.

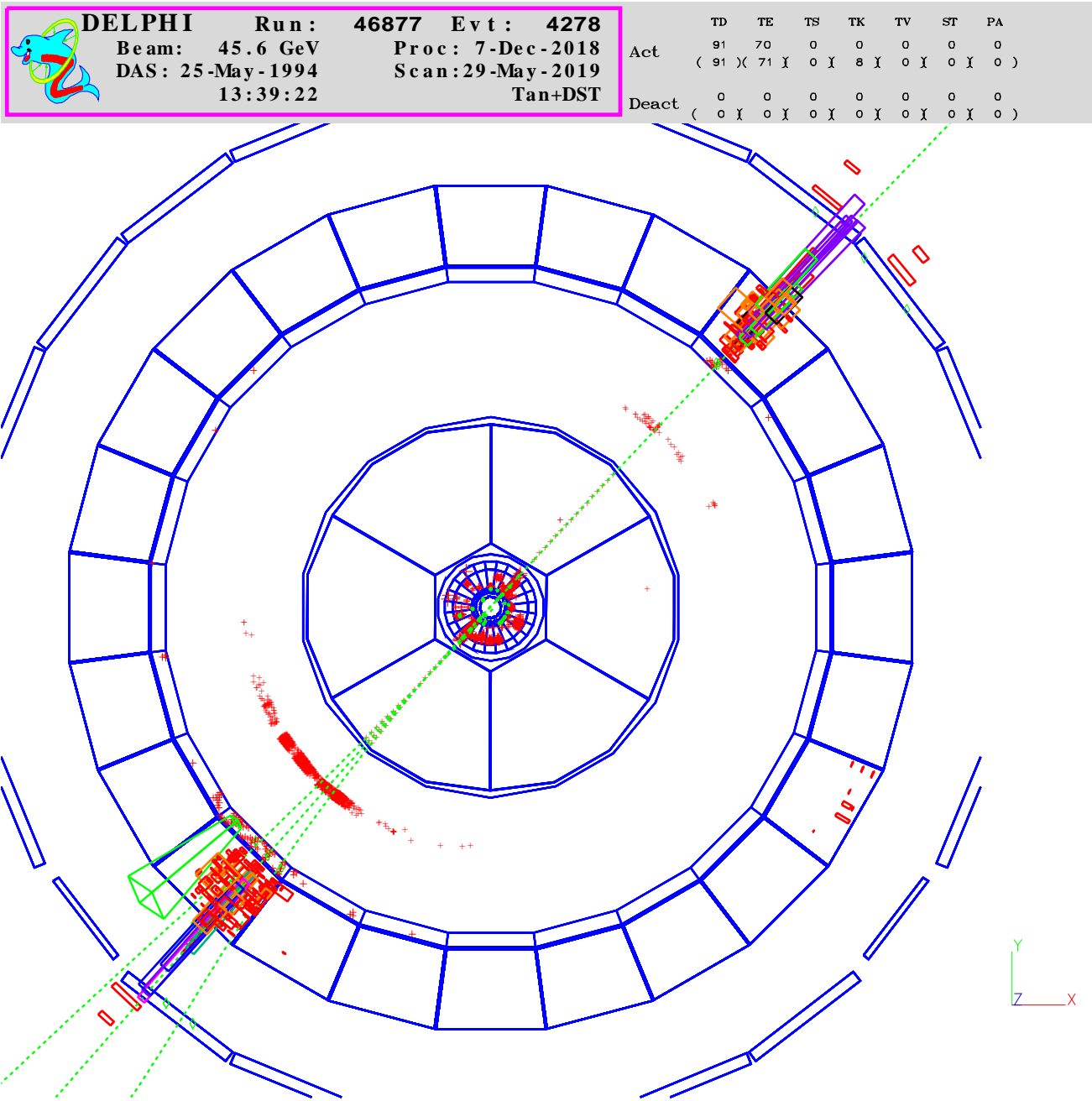


Figure 17: An event of topology 3, a general view.

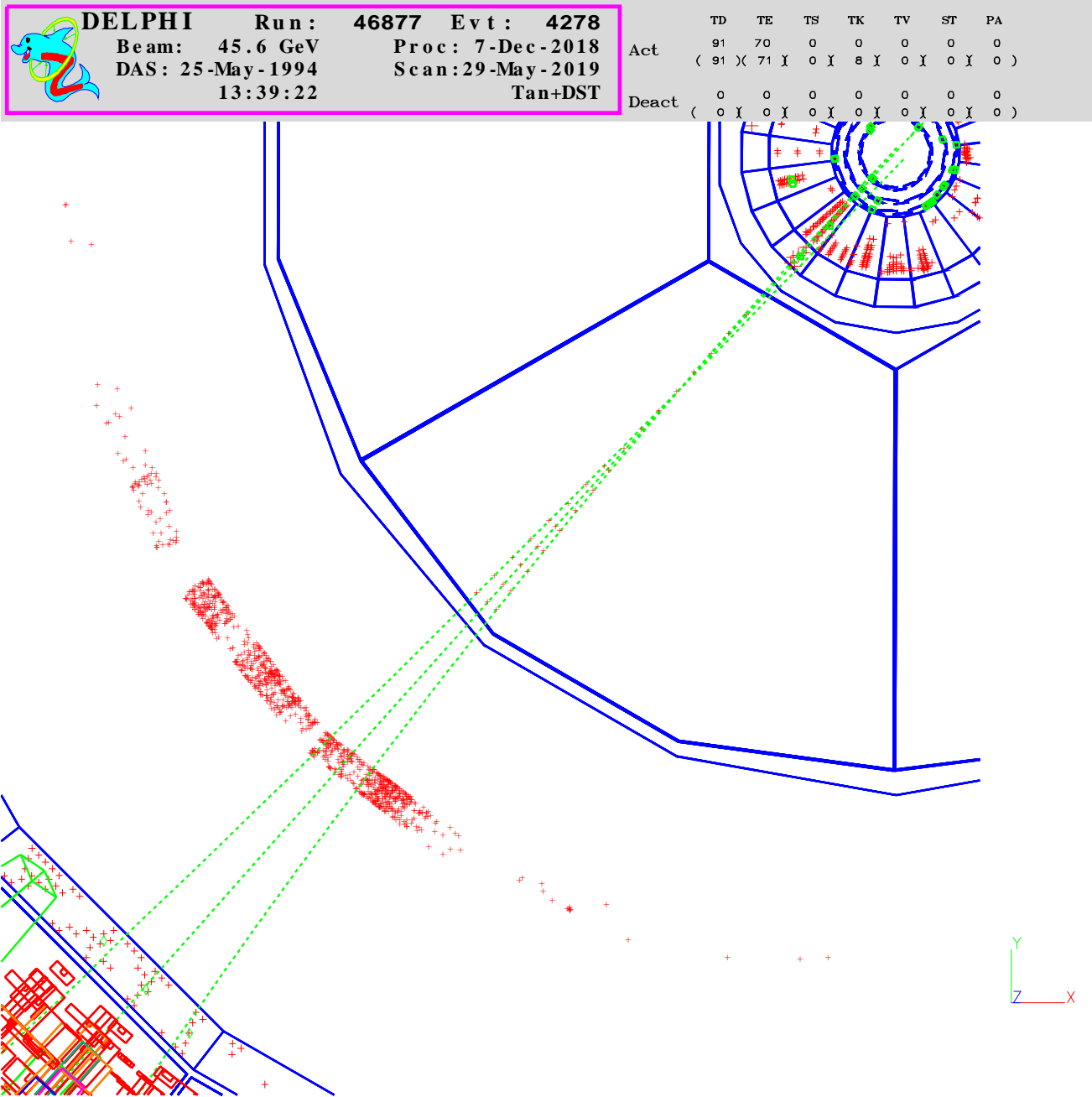


Figure 18: The same event, the 3-particle jet view.

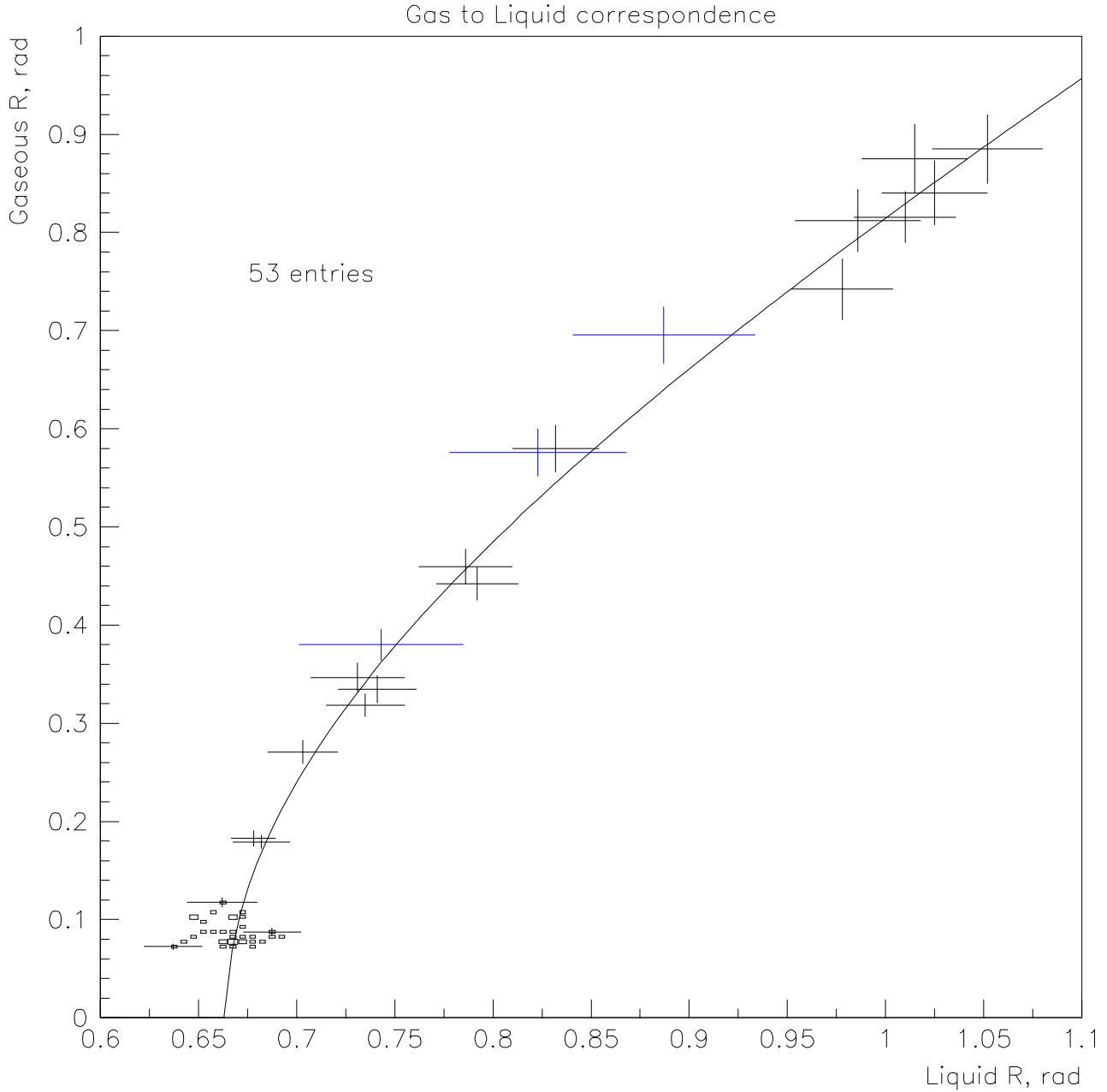


Figure 19: Radii of the anomalous rings expressed in angular units as measured in the liquid and in the gaseous radiators. The curved line shows the expected theoretical correspondence between the radii in the two radiators given by the formula  $n_{liq} \cos \theta_{liq} = n_{gas} \cos \theta_{gas}$ , with  $n_{liq} = 1.273$  and  $n_{gas} = 1.00194$ . The errors in the left bottom corner are suppressed to avoid pile-up; only several crosses are left in order to present a typical angular error in this region; 5 boxes of the area twice as big as that of the rest boxes in this corner represent double entries. 3 crosses drawn in dark blue correspond to anomalous rings coming from the quartz radiator. Their radii are recalculated to the liquid ring radii taking into account the difference of the corresponding refraction indices. For presentation purposes the scale along the  $x$  axis is made two times finer than that of the  $y$  axis.

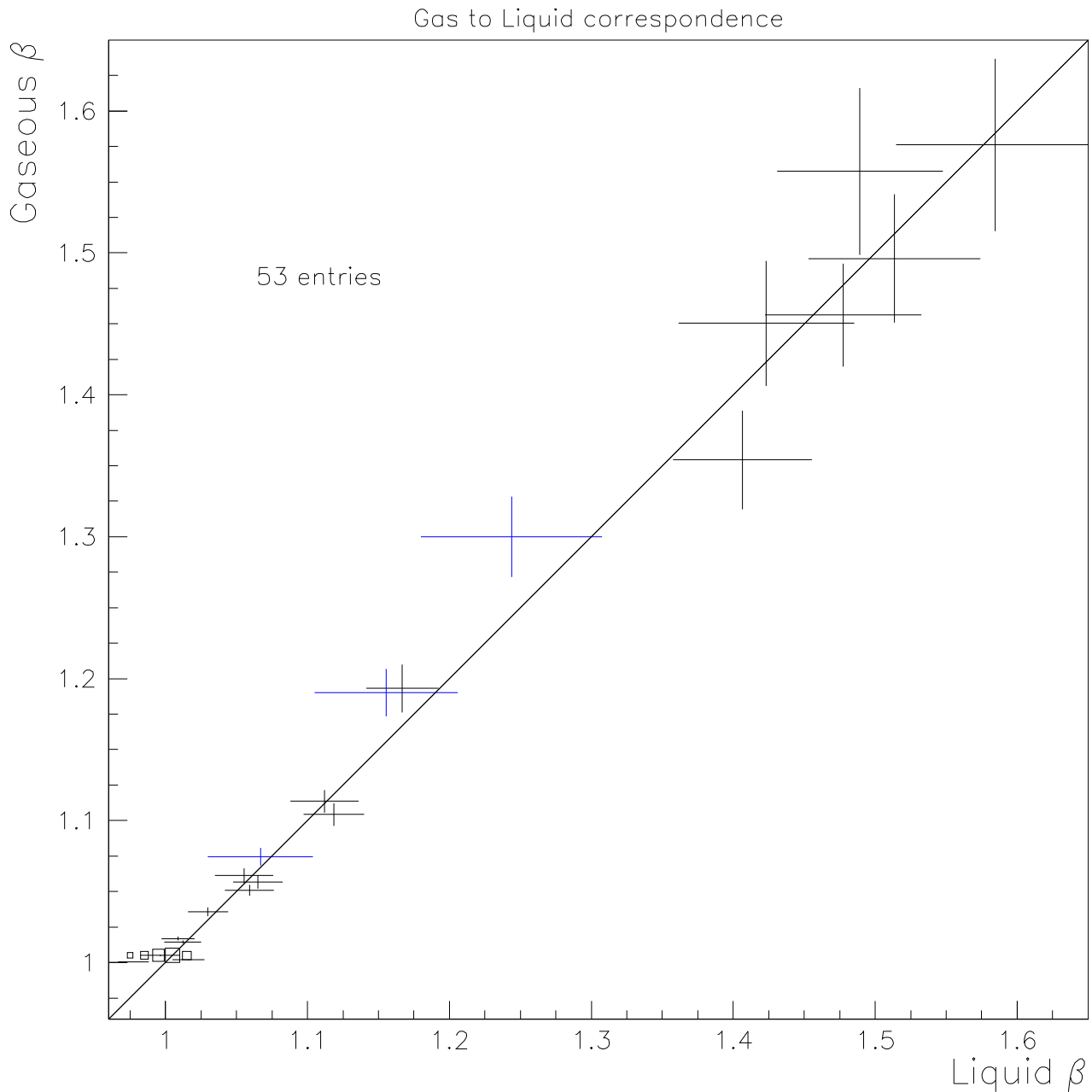


Figure 20: Particle velocities ( $\beta = v/c$ ) corresponding to radii of the anomalous rings as measured in the liquid and in the gaseous radiators. The diagonal indicates where the values of the two variables  $\beta_{liq}$  and  $\beta_{gas}$  are equal. 3 crosses drawn in dark blue correspond to anomalous rings coming from the quartz radiator (see caption to Fig. 19). The correlation coefficient for the points in this plot is 0.992. The sum of  $\chi^2$  for the deviations of the 53 points from the diagonal is 40.1. The corresponding p-value for the points to be consistent with the diagonal is near 95%.

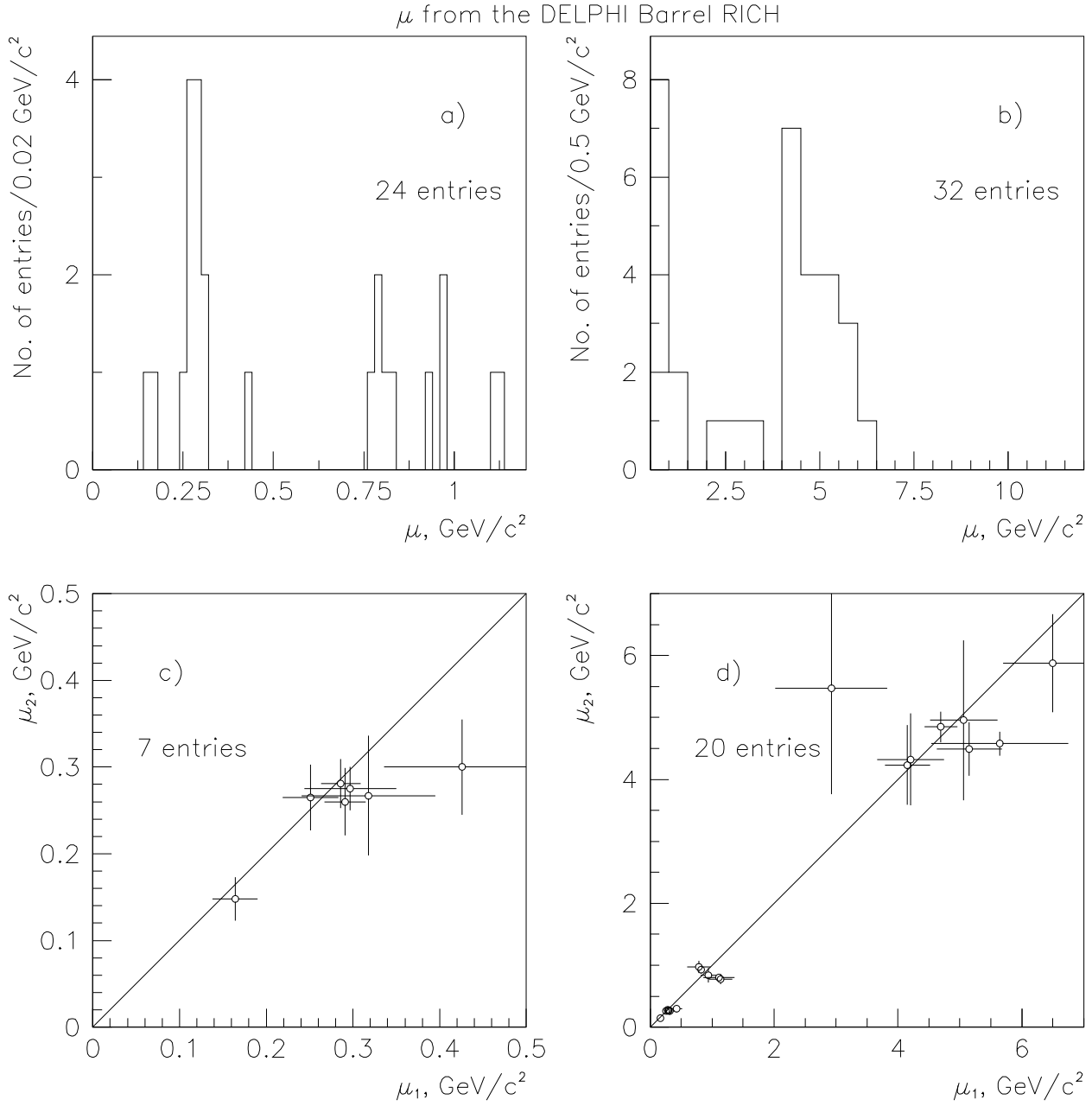


Figure 21: **a)** The distribution of the tachyon mass parameters as calculated from the measured Cherenkov angles and the track momenta, low mass parameter region; **b)** The same for a high mass parameter region; **c)** Two-dimensional plot of tachyon mass parameters for events in which both tachyon candidate track momenta were measured, low mass parameter region; **d)** The same for the overall mass parameter region. The diagonals in panels **c)** and **d)** indicate where the values of the two variables  $\mu_1$  and  $\mu_2$  are equal.

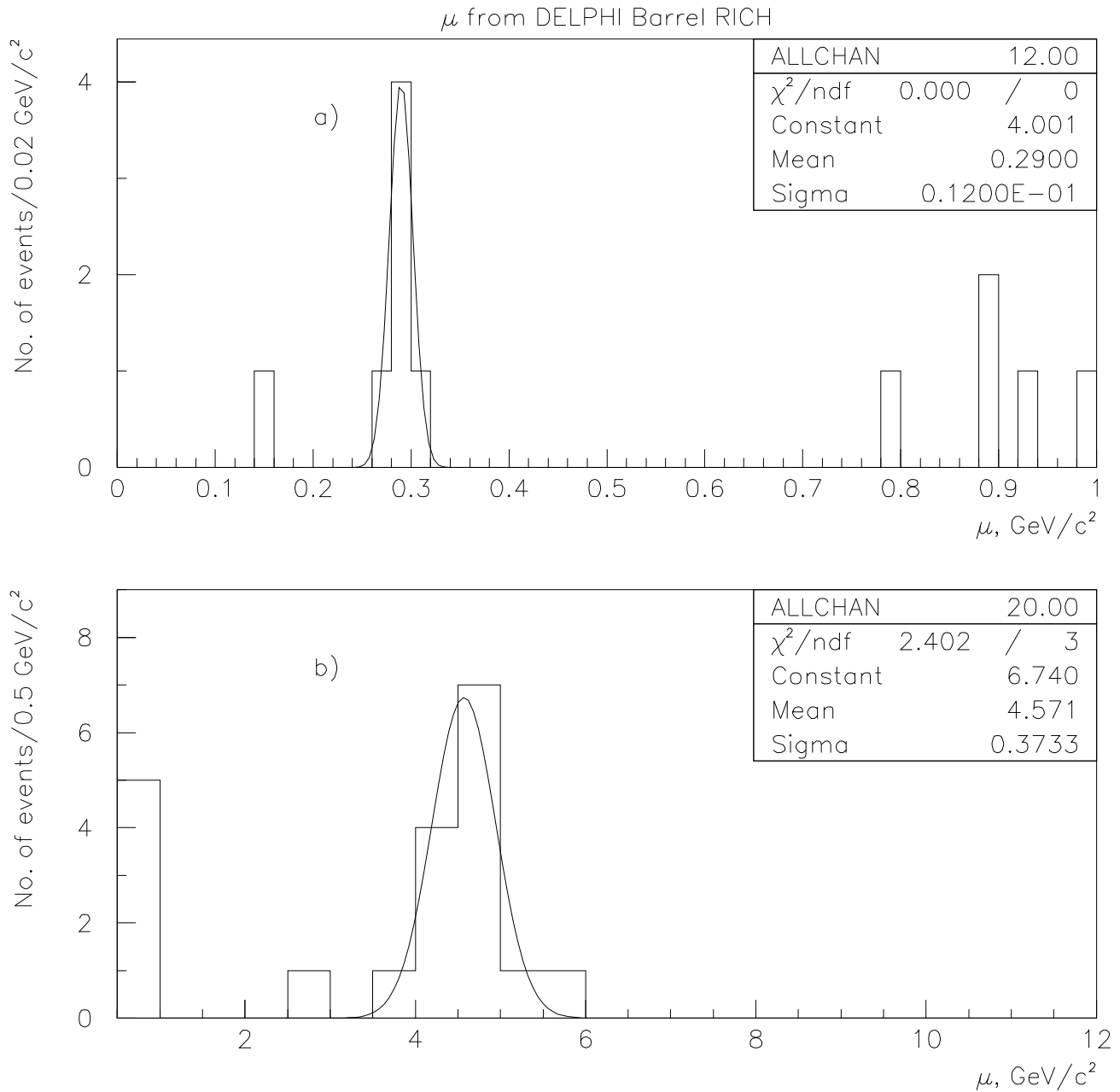


Figure 22: The distribution of the tachyon mass parameters obtained with events containing anomalous rings and passed kinematic fits: **a)** in the mass region below  $1 \text{ GeV}/c^2$  (to be compared with Fig. 21a). The curve presents the result of a fit of the peak at  $0.29 \text{ GeV}/c^2$  by a Gaussian; **b)** an analogous tachyon mass parameter distribution in the high mass region, the low mass region (below  $0.5 \text{ GeV}/c^2$ ) being excluded (to be compared with Fig. 21b). The curve presents the result of a fit of the peak at  $4.5 \text{ GeV}/c^2$  by a Gaussian.